Estimating the Efficiency of Cell Capture and Arrest in Flow Chambers: Study of Neutrophil Binding via E-selectin and ICAM-1

Yi Zhang and Sriram Neelamegham
Bioengineering Laboratory, Department of Chemical Engineering, State University of New York at Buffalo, Buffalo, New York 14260 USA

ABSTRACT A mathematical model was developed to quantify the efficiency of cell–substrate attachment in the parallel-plate flow chamber. The model decouples the physical features of the system that affect cell–substrate collision rates from the biological features that influence cellular adhesivity. Thus, experimental data on cell rolling and adhesion density are converted into "frequency" parameters that quantify the "efficiency" with which cells in the flow chamber progress from the free stream to rolling, and transition from rolling to firm arrest. The model was partially validated by comparing simulation results with experiments where neutrophils rolled and adhered onto substrates composed of cotransfected cells bearing E-selectin and intercellular adhesion molecule-1 (ICAM-1). Results suggest that: 1) Neutrophils contact the E-selectin substrate on average for 4–8.5s before tethering. This contact duration is insensitive to applied shear stress. 2) At 2 dyn/cm^2, ~28% of the collisions between the cells and substrate result in primary capture. Also, ~5–7% of collisions between neutrophils in the free stream and previously recruited neutrophils bound on the substrate result in secondary capture. These percentages were higher at lower shears. 3) An adherent cell may influence the flow streams in its vicinity up to a distance of 2.5 cell diameters away. 4) Our estimates of selectin on-rate in cellular systems compare favorably with data from reconstituted systems with immobilized soluble E-selectin. In magnitude, the observed on-rates occur in the order, L-selectin > P-selectin > E-selectin.

GLOSSARY

Note: All vector quantities are in bold. Variables with asterisk in superscript are in dimensionless form.

$u\|_{y=m}$	value of the variable u at position $y = m$.
a, a_e	cell radius, radius of receptor–ligand encounter complex
A, A_{-1}, A_{tot}	adhesion flux, adhesion release flux, total adherent cell density
b	half chamber height
C, C_b	cell concentration per unit volume at any point, at the inlet of the flow chamber
C_r	rolling cell concentration per unit area
C_L	ligand concentration per unit substrate area
C_1, C_2, C_3, C_4	intermediate constants
D	relative diffusion coefficient
f_{max}	fraction of substrate area occupied by cells at maximum density
$\mathbf{G}$	velocity gradient tensor
i, j	grid element number in x and y direction
k_{ad}, k_f,	adhesion rate constant, forward rate
k_{in}, k_{on}	constant, intrinsic reaction rate constant, lumped on-rate
L	length of flow chamber
m, m_1, n	grid number in y direction for R2a, for R2b, grid number in x direction.
Nu, Pe	Nusselt number, Peclet number
N_{col}	total number of cell–substrate collisions per unit time over the entire flow chamber area
N_R	receptor number in contact region
P	capture probability
Q	flow rate
r	radial distance
R, R_P,	total tethering flux, primary tethering flux,
R_S, R_{-1}	secondary tethering flux, rolling-release flux
t, $t_{1/2}$	time, average time
t_e	receptor–ligand encounter duration
u_r, u_f, u_{max}	rolling velocity, free stream velocity, maximum free stream velocity
v_{set}, v^o_{set}	actual settling velocity, free settling velocity
$\mathbf{V}$	relative velocity between cell surface and substrate
v_x, v_y, v_z,	flow velocity in Cartesian and spherical coordinates
v_r, v_θ, v_ϕ	
w	flow chamber width
x_0, y_0	coordinate at which cells enter flow chamber
Z_{cc}	secondary collision frequency per unit substrate area

Greek symbols

λ	cell microvillus length
μ, ρ_c, ρ_m	fluid viscosity, cell density, medium density
γ_w,τ_w	wall shear rate, wall shear stress
Ω	angular velocity of the cell
θ_{fr}, θ_{ra}, θ_{rf},	primary capture frequency, firm-arrest frequency, rolling-release frequency,
θ_{ar}, θ_{cc}	adhesion-release frequency, cell–cell capture probability

Submitted March 12, 2002 and accepted for publication June 20, 2002.

Address reprint requests to Sriram Neelamegham, Dept. of Chemical Engineering, 906 Furnas Hall, SUNY at Buffalo, Buffalo, NY 14260. Tel.: 716-645-2911 x2220; Fax: 716-645-3822; E-mail: neel@eng.buffalo.edu.

0006-3495/02/10/1934/19 $2.00

INTRODUCTION

The parallel-plate flow chamber is used to study the biophysics of receptor–ligand interactions under physiologically relevant hydrodynamic flow conditions. This system has been applied to quantify the kinetics of leukocyte/bead binding to reconstituted ligand-coated substrates, activated endothelial cells, platelets, and other leukocytes (Diacovo et al., 1996; King and Hammer, 2001; Lawrence et al., 1987; Walcheck et al., 1996). It has also been used to quantify the progress and mechanism of processes like cancer metastasis and bacterial infection (Felding-Habermann et al., 1996; Mohamed et al., 1999).

Typically, studies carried out in the flow chamber have quantified the interactions between the cells and substrate in terms of the number of rolling cells and the number of adherent cells per unit area (Lawrence et al., 1987; Puri et al., 1997). Besides the biological adhesivity of cells, these measures are also functions of the physical features that affect the rate of cell–substrate interactions including the cell and media density, cell radius, inlet cell concentration, dimensions of the flow chamber, and the applied shear rate/stress (Munn et al., 1994; Patil et al., 2001; Rinker et al., 2001). For example, changing the cell concentration between runs dramatically alters the number of rolling cells by influencing the number of cell–substrate and cell–cell collisions. Also, in experiments that compare the rolling behavior of different cell types (e.g., neutrophils versus lymphocytes) the cell's physical properties, especially density and size, may play an important role in controlling the rate of cell–substrate collision. An understanding of the parameters controlling the number of rolling cells is important because it directly influences the number of adherent cells. To further complicate the issue, once the first few cells are rolling on the ligand–coated substrate, binding interactions between the rolling cells and cells in the free stream may also influence the rate of cell recruitment (Alon et al., 1996; Walcheck et al., 1996). Because of these issues, data from different laboratories or even different treatments cannot be readily compared.

The focus of the current paper is on neutrophil binding to substrates bearing adhesion molecules from the selectin and immunoglobulin supergene family. Specifically, we examine the multi-step process of cell adhesion to E-selectin and intercellular adhesion molecule-1 (ICAM-1) (Gopalan et al., 1997; Simon et al., 2000), because this type of cell recruitment provides a model system to study inflammatory diseases. In this adhesion process, endothelial E-selectin supports neutrophil capture and rolling (Abbassi et al., 1993), whereas following cellular activation firm arrest is mediated by the β_2-integrins (Simon et al., 2000). The β_2-integrins bind ICAM-1 and other ligands on the substrate.

To delineate between the role of fluid flow in controlling the flux of cells to the substrate and its role in modulating molecular bonding, we propose to analyze flow-chamber data using a kinetic model. The current work is similar to previous work by Munn et al. (1994) in that we assume that the flux of cells to the substrate is dependent on cell settling and convection velocities. However, whereas the focus of the previous paper was only on predicting the flux of cells to the substrate, we also predict the effect of this cell–substrate collision on the time-dependent evolution of cell rolling and adhesion densities in the flow chamber. Further, we account for lubrication effects near the plate surface (Brenner, 1961) and incorporate the role of cell microvilli in controlling adhesion rates.

Here, a series of first-order partial differential equations are set up to quantify the steady- and unsteady-state flux corresponding to the cells in the free stream, the rolling cells, and the firmly adherent cells. Frequency parameters are also introduced to measure the different interactions in the cell adhesion system: the capture of cells from the free stream onto the substrate to initiate rolling is quantified using the *primary capture frequency*, the transition from cell rolling to arrest is measured by the *firm-arrest frequency*, and the fraction of collisions between cells in the flow stream and surface-bound cells that result in the initiation of cell rolling is quantified using the *cell–cell capture probability*. Other parameters are also introduced to account for the release of cells from rolling and firm arrest. These model parameters are independent of each other. They are functions of the biological properties that influence the adhesivity of cells, including the number of receptors and ligands, their affinity, topography, activation levels and their response to applied forces. We apply the model to distinguish between cell–substrate binding events (primary capture) and cell–cell binding (secondary capture). We also estimate the on-rates of selectin bonds based on previously published data (Puri et al., 1997). Although the current paper studies selectin, integrin, and immunoglobulin-mediated neutrophil adhesion in a model of inflammation, the proposed analysis methodology may be applied to other experimental systems also.

MATHEMATICAL MODELING

Trajectory of cells

The parallel-plate flow chamber has a defined flow profile that simulates the features of hydrodynamic forces found in the vasculature. A typical device consists of two parallel plates separated by a gasket. The thickness of the gasket controls the height of the flow chamber (Fig. 1). The bottom plate of the chamber is composed of either glass or plastic. It bears a ligand-expressing substrate, typically adsorbed extra-cellular matrix proteins, adhesion molecule-bearing cells, or isolated ligand molecules. A syringe pump precisely controls the flow rate of the cell suspension over the substrate. Cells entering the flow chamber interact with this ligand-bearing substrate as depicted in Fig. 1 *A*. In this apparatus, the wall shear rate

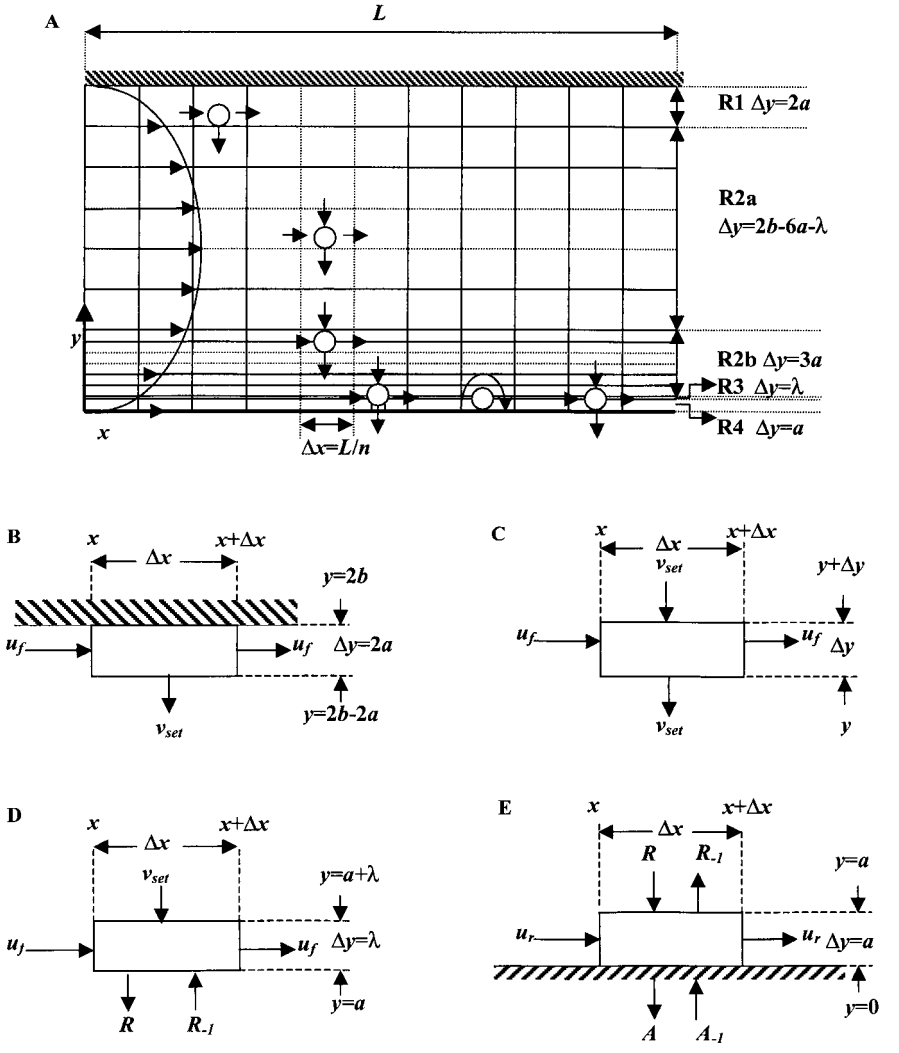

FIGURE 1 Regions of the parallel-plate flow chamber. (*A*) The flow chamber of length L and height $2b$ is divided into n uniform divisions in the x direction and $(m + m_1 + 3)$ divisions in the y direction. Cells entering the chamber both convect with a velocity u_f and settle at v_{set}. Upon reaching the substrate, the cells may undergo rolling or firm-adhesion. The flow chamber is divided into four regions, labeled Region 1 (R1) to Region 4 (R4). (*B*) Mass flux in R1. The height of this region equals the cell diameter $2a$. Cells enter by convection and leave either via convection or settling. (*C*) Mass flux in R2. R2 is divided into two sections: R2a consisting of m coarse divisions and R2b with m_1 finer divisions. Cells enter this region either via convection or settling. In most cases, they leave the grid element via the same mechanisms. The exceptions to this are the bottom rows of R2b ($3a + \lambda > y \geq a + \lambda$) where secondary capture may also contribute to cell efflux. (*D*) Mass flux in R3. This region is of height λ, the cell microvillus length. In addition to settling and convection, the tethering of cells at a rate R and the release of rolling cells at a rate R_{-1} also control the mass flux here. (*E*) Mass flux in R4. Adhesion flux (A) and adhesion-release rate (A_{-1}) are also important in this region. The cell rolling velocity is denoted u_r.

(γ_w) is related to the flow rate of the syringe pump (Q), the chamber height ($2b$, equal to the thickness of the gasket) and flow section width (w) by the relation $\gamma_w = 3Q/2b^2w$. The wall shear stress τ_w for a Newtonian fluid with viscosity μ is then defined as $\tau_w = \mu\gamma_w$.

Cells entering the flow chamber experience two types of forces: the force of gravity, which causes them to settle with a velocity v_{set} along the y axis, and the fluid convective force in the x direction, which causes them to translate axially with a velocity, u_f (Munn et al., 1994). When the cell is far from the flow chamber substrate, we assume that the cell is freely settling with a velocity v^o_{set} expressed by Stokes' equation,

$$v^o_{set} = \frac{2}{9}(\rho_c - \rho_m)g\frac{a^2}{\mu}, \tag{1}$$

where a is the cell radius, ρ_c is the cell density, and ρ_m is the media density. When close to the plate surface, however, the settling speed is less than the free settling velocity because of lubrication effects (Brenner, 1961). This reduction in settling velocity occurs because of balance between two opposing forces: the forces of gravity that drive the particle to the surface and the lubrication layer between the particle and the substrate that resists this motion. Overall, the settling velocity, v_{set}, at any point in the flow chamber is expressed as a function of y, the distance from the substrate to the cell's center. The exact solution of this problem is well approximated by (Davis and Giddings, 1985)

$$v_{set} \approx \frac{v^o_{set}}{1 + a/(y - a)}. \tag{2}$$

Here, $(y - a)$ denotes the separation distance between the cell and the substrate. The convection velocity of the cells in the free stream varies quadratically with height from the substrate

as described below, where u_{max} is the maximum convection velocity at the center of the flow chamber (Fig. 1),

$$u_f = \frac{3Q}{4b^3w}(2by - y^2)$$

$$= \frac{u_{max}}{b^2}(2by - y^2). \quad (3a)$$

Close to the plate surface (at approximately $y < 4a$), the convection velocity is reduced by hydrodynamic wall effects. Exact results for u_f (Goldman et al., 1967) are well approximated by the far-field asymptotic formula,

$$u_f \approx y\gamma_w\left(1 - \frac{5}{16}\left(\frac{a}{y}\right)^3\right). \quad (3b)$$

The equations of settling (Eq. 2) and convection (either Eq. 3a or 3b depending on the y-coordinate) can be combined to yield an equation that describes the (x, y) trajectory of a cell that enters the flow chamber at an initial coordinate (x_0, y_0). For example, above $y = 4a$, Eqs. 2 and 3a combine to give the trajectory equation (Eq.4). A similar equation can be derived by combining Eq. 2 and 3b for $y < 4a$.

$$x - x_0 = \frac{u_{max}}{b^2\nu^o_{set}}\left(\frac{y^3 - y_0^3}{3} + \frac{(a - 2b)(y^2 - y_0^2)}{2} + (a^2 - 2ab)(y - y_0) + (a^3 - 2a^2b)\ln\frac{y - a}{y_0 - a}\right) \quad (4)$$

Number of cell–substrate collisions

The cells are modeled to be spheres of radius a with microvilli protrusions of length λ. Thus, the tips of the microvilli contact the substrate when the cell is at a height $y = a + \lambda$. In the case of leukocytes, several families of adhesion molecules, including the selectins and their major ligands (Erlandsen et al., 1993; Moore et al., 1995), are found localized at the tips of microvilli. Thus, cell recruitment may occur after the cells settle to a height, $y = a + \lambda$.

To determine the total number of cell–substrate collisions per unit time (N_{col}) over the entire flow chamber area at a given shear rate, we determined a parameter called the critical y coordinate, y_{crit}. This is the largest y coordinate at the inlet of the flow chamber where the cell must enter if it is to just touch the chamber substrate before exiting the device at $(x, y) = (L, a + \lambda)$. All cells that enter the flow chamber below y_{crit} thus collide with the substrate and contribute to N_{col}. When cells at a concentration C_b enter a flow chamber with width, w, we thus define

$$N_{col} = \int_{a+\lambda}^{y_{crit}} C_b u_f w \, dy. \quad (5)$$

The efficiency of adhesion in the flow chamber

All the cells observed in the flow-chamber are either in the free stream, rolling on the plate surface, or firmly adherent on the substrate. For the purpose of solving the concentration of cells in various regions of the flow chamber, we divide the apparatus using a two-dimensional (2D) mesh in the x and y direction (Fig. 1). There are n equal-sized divisions in the x direction. In the vertical y direction, there are $m + m_1 + 3$ divisions. Greater resolution is provided at the bottom of the flow chamber to more carefully resolve between the rolling cells and those in the free stream near the substrate. Each of the elements of the mesh is said to be located in one of 4 "regions" depicted from R1 to R4 (Fig. 1) depending on the nature of cell accumulation and the mass balance equation. A description of each Region follows.

Region 1 or R1 ($2b > y \geq 2b - 2a$, Fig. 1 *B*) is the topmost row of the flow chamber. In each mesh element of this region, cells enter by convection from the previous element and they leave either by convection to the right or by settling below. Together, these rates determine the cell concentration C (cells/volume) at any point (x, y) and time t:

$$\frac{\partial C}{\partial t} = -\frac{\nu_{set}|_{y=2b-a}}{2a}C - u_f|_{y=2b-a}\frac{\partial C}{\partial x}. \quad (6)$$

The initial (IC) and boundary (BC) condition required for the solution are

$$\begin{array}{lll} \text{IC} & C = 0 & \text{at} \quad t = 0, \\ \text{BC} & C = C_b & \text{at} \quad x = 0. \end{array}$$

Writing the above equations in dimensionless form using $C^* = C/C_b$, $t^* = \nu^o_{set}t/(2b)$, $x^* = x/L$ and $v^*_{set} = v_{set}/\nu^o_{set}$, we get

$$\frac{\partial C^*}{\partial t^*} = -\frac{b\nu^*_{set}|_{y=2b-a}}{a}C^* - \frac{2bu_f|_{y=2b-a}}{\nu^o_{set}L}\frac{\partial C^*}{\partial x^*},$$

$$\begin{array}{lll} \text{IC} & C^* = 0 & \text{at} \quad t^* = 0, \\ \text{BC} & C^* = 1 & \text{at} \quad x^* = 0. \end{array} \quad (7)$$

The analytical solution of the above first-order partial differential equation is

$$C^* = \begin{cases} \exp\left(-\dfrac{\nu^o_{set}Lb^2(b - a)}{a^2(2b - a)^2u_{max}}x^*\right) & \tau^*_1 > 0, \\ 0 & \tau^*_1 < 0, \end{cases} \quad (8)$$

where $\tau^*_1 = 2a(2b - a)u_{max}t^*/(\nu^o_{set}Lb) - x^*$.

Region 2 or R2 ($2b - 2a > y \geq a + \lambda$, Fig. 1 *C*) constitutes the bulk of the flow chamber between the upper and lower surface. This region is subdivided into two parts: Region 2a (R2a) has m coarse divisions that cover the flow chamber volume four cell radii above the substrate ($2b - 2a > y \geq 4a + \lambda$), and Region 2b (R2b) has m_1 finer divisions that cover the sections within 4 cell radii of the substrate ($4a + \lambda > y \geq a + \lambda$). In our simulations, m was set to 11 and m_1 to 25. Cells enter R2 (either R2a or R2b) either by settling from the mesh element above or via convection from the previous element. They leave the element in a similar fashion. A mass balance equation for any element in this region is

$$\frac{\partial C^*}{\partial t^*} = \frac{\partial(\nu^*_{set} C^*)}{\partial y^*} - \frac{2bu_{max}}{\nu^o_{set} L} u^*_f \frac{\partial C^*}{\partial x^*},$$

$$\begin{array}{lll} \text{IC} & C^* = 0 & \text{at } t^* = 0, \\ \text{BC1} & C^* = 1 & \text{at } x^* = 0, \\ \text{BC2} & C^* \text{ from Eq. 8} & \text{at } y = 2b - 2a. \end{array} \quad (9a)$$

Note that additional dimensionless parameters, $y^* = y/2b$ and $u^*_f = u_f/u_{max}$, have been introduced here.

We note here that some cells at the bottom section of R2b that are less than 1.5 cell diameter from the substrate (i.e., at $3a + \lambda > y \geq a + \lambda$) may contact already adherent cells and thus tether via "secondary capture mechanism" (Alon et al., 1996; Mitchell et al., 2000). The mass balance in this bottom region of R2b thus includes an additional efflux term to account for secondary capture (Eq. 9b). We describe this secondary tethering mechanism and the mathematical form of R^*_S in more detail in the next section.

$$\frac{\partial C^*}{\partial t^*} = \frac{\partial(\nu^*_{set} C^*)}{\partial y^*} - \frac{2bu_{max}}{\nu^o_{set} L} u^*_f \frac{\partial C^*}{\partial x^*} - \frac{R^*_S}{\Delta^*_y}. \quad (9b)$$

Here, $R^*_S = R_S/C_b\nu^0_{set}$ and $\Delta y^* = (3a/(m_1 - 1))/(2b)$. R_S is the tethering flux due to secondary capture in unit of cells/area/time. Unlike the equations for R1, Eq. 9 does not have an analytical solution. It is solved using finite difference as described later.

Region 3 or R3 ($a + \lambda > y \geq a$, Fig. 1 *D*) is a region of height equal to the cell microvillus length, λ. It represents the lowest layer of the flow chamber with convective mass flow. In this region, cells come in contact with the substrate. They enter R3 either via convection from the previous element or by settling from above. In addition to exiting the element by convection to the next element, these cells may also bind or "tether" onto the ligand-coated substrate. Tethering marks the capture of cells from the flow stream onto the chamber substrate and this initiates cell rolling.

Two mechanisms may contribute to the tethering of cells: Adhesion molecules on the cell surface may bind ligands expressed by the flow chamber substrate. This process is termed "primary capture." Free-flowing cells may interact with previously recruited cells, and this may contribute to new tethering events through a "secondary capture" process. In this case, the previously recruited cells may either directly present ligands for cell capture, or they may alter the local hydrodynamic environment near the substrate, thus changing the rate of cell–substrate attachment.

In this model, to quantify these two modes of cell recruitment, we introduce the terms "primary capture frequency", θ_{fr} (unit of length^{-1}), and "cell–cell capture probability", θ_{cc} (dimensionless unit). The primary capture frequency is analogous to a first-order reaction rate constant, and is defined as

$$R_P = \theta_{fr}\lambda u_f\big|_{y=a+\lambda/2} C\big|_{y=R3}. \quad (10)$$

In this equation, the rate of primary capture, denoted by the primary tethering flux R_P (unit of cells captured/area/time) is directly proportional to the local cell concentration in R3. Further, analogous to a first-order reaction with rate constant k, where the half-life of a reaction is given by $\ln(2)/k$, it can be shown that the average distance the cell traverses in region R3 before primary capture equals $\ln(2)/\theta_{fr}$. The time taken to travel this distance ($t_{1/2}$) is thus $\ln(2)/(\theta_{fr}\, u_f)$.

Cell–cell capture probability θ_{cc} is a measure of the fraction of collisions between cells in the free-stream and previously adherent cells that result in capture. This is analogous to cell–cell adhesion efficiency, which we have used elsewhere to quantify cellular binding kinetics in suspension (Neelamegham et al., 1997b). The cell tethering flux due to secondary capture, R_S (unit of cells captured/area/time), is a product of cell–cell capture probability and the frequency with which cells in the free stream collide with already bound cells, Z_{cc} (collisions/area/time):

$$R_S = \theta_{cc} Z_{cc} = \theta_{cc}(C_r + A_{tot}) \iint_S \nu_x C \, dA. \quad (11)$$

To estimate Z_{cc}, we calculate the number of particles entering a "collision sphere" around a surface bound cell (Fig. 2). This collision sphere is an imaginary sphere (with radius = $2a$) surrounding the surface-adherent cell. If the center of any other particle enters this collision sphere, cell–cell collision occurs. The term in the integral (Eq.11) denotes the total number of collisions taking place with any given adherent cell. Here, dA represents the projected area of an element of the collision sphere surface on the yz-plane (Fig. 2) and v_x (calculated from Eq. A5, Appendix) is the local free stream velocity along the x-direction at that point. The cell in the free stream may interact with either the rolling or firmly adherent cells on the substrate. This accounts for the factor $C_r + A_{tot}$. Here, A_{tot} is the density of adherent cells (cells/unit area) and C_r denotes the number of rolling cells

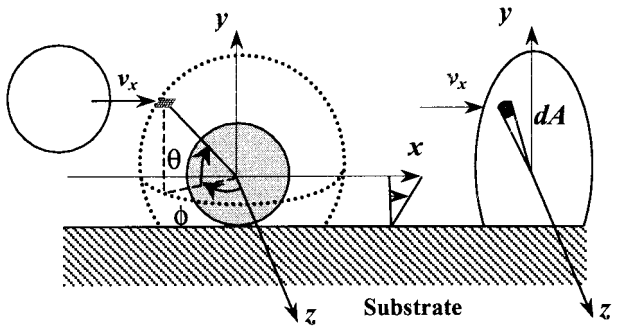

FIGURE 2 Estimating secondary tethering flux (R_S). The schematic represents a dotted collision sphere of radius $2a$ surrounding a surface-bound cell (*gray*). If the center of any other cell enters this collision sphere, cell–cell collision occurs. The number of cell–cell collisions is estimated by calculating the mass flux of cells into the collision sphere (Eq. 11). *dA* depicts the projection of an area element located on the collision sphere surface at $(2a, \phi, \theta)$ onto the *yz*-plane.

per unit area. Methods to determine A_{tot} and C_r are described in the next section.

The total tethering flux can be estimated by summing R_P and R_S when the density of rolling cells is low, i.e., during the initial phases of the experiment. However, it is evident that, at the later time points when a substantial fraction of the substrate area is occupied, the rate of cell attachment is lower, and it is never possible to completely pack the ligand-bearing substrate with rolling cells. To account for this feature, in the model, we introduce a parameter f_{max}, defined as the fraction of the substrate surface area ($L \cdot w$) that is occupied when the substrate coverage reaches maximum. Assuming a linear relationship between tethering flux ($R_P + R_S$) and the substrate area available for cell recruitment, we thus determine an expression for the total tethering flux, R (Eq.12). Although we experimentally estimated f_{max} to be 0.025 in our system where neutrophils bound substrates bearing cotransfected cells, we note that this parameter may be higher in other systems, especially when cells bind to reconstituted ligand-bearing substrates,

$$R = (R_P + R_S) \times \left(1 - \frac{\pi a^2 (C_r + A_{tot})}{f_{max}}\right). \qquad (12)$$

Under some conditions where the off-rate of ligands is high or when the ligand density is sparse, some of the rolling cells may "release" from the surface and change back to the free stream. The flux of this transition is denoted by R_{-1} (number of cells release from rolling/area/time),

$$R_{-1} = \theta_{rf} u_r C_r. \qquad (13)$$

In this equation, the rate at which rolling cells are released to the free stream is quantified using a "rolling-release frequency", θ_{rf} (units of length^{-1}). This parameter is analogous to a first-order rate constant. From a physical standpoint, the average cell can be thought to roll a distance equal to $\ln(2)/\theta_r$ before moving back into the free stream.

If we set $R^* = R/C_b\nu^0_{set}$ and $R^*_{-1} = R_{-1}/C_b\nu^o_{set}$, the dimensionless form of the mass balance equation for R3 follows (Eq. 14). Solution of this equation yields an estimate of the cell concentration in R3.

$$\frac{\partial C^*}{\partial t^*} = \frac{2b}{a+\lambda} C^* + \frac{2b}{\lambda}(R^*_{-1} - R^*) - \frac{2bu_f}{\nu^o_{set} L}\frac{\partial C^*}{\partial x^*},$$

$$\begin{array}{lll} \text{IC} & C^* = 0, & \text{at } t^* = 0, \\ \text{BC1} & C^* = 1, & \text{at } x^* = 0 \\ \text{BC2} & C^* \text{ from Eq. 9} & \text{at } y = a + \lambda. \end{array} \qquad (14)$$

Region 4 or R4 ($a > y$, Fig. 1 *E*) is the region of the flow chamber with the rolling cells. Although cells enter and leave this region by the fluxes described by R (Eq.10–12) and R_{-1} (Eq.13), the rate of firm adhesion also regulates the number of rolling cells. The rate of this arrest process, which is estimated by the adhesion flux parameter, A (number of adherent cells/area/time), is directly dependent on the number of rolling cells according to

$$A = \theta_{ra} u_r C_r. \qquad (15)$$

Here, u_r is the cell rolling velocity. The frequency with which rolling cells change to firm-adhesion is quantified using the "firm-arrest frequency", θ_{ra} (length^{-1}). Analogous to the frequency parameters described above, $\ln(2)/\theta_{ra}$ is the average distance that the cell rolls before it switches to firm arrest on the substrate. The time taken for such a transition for an average cell equals $\ln(2)/(\theta_{ra}\, u_r)$.

Similar to the release of rolling cells from the substrate, adherent cells may also be released back as rolling cells. To describe this phenomena, "adhesion-release frequency", θ_{ar} (units of time^{-1}), is introduced. The rate of adhesion–release A_{-1} (number of cells release/area/time) is set to equal the product of θ_{ar} and the total adherent cells, A_{tot} (number of adherent cells/area),

$$A_{-1} = \theta_{ar} A_{tot}. \qquad (16)$$

We note here that it is possible that cells that are previously adherent may be released directly into the free stream, instead of rolling, in which case, similar modifications can be made to the model. The density of adherent cells at any time is based on the cumulative adhesion and release of cells over the time course of the experiment. At any time t, it is mathematically expressed as

$$A_{tot} = \sum_{time=0}^{t} (A - A_{-1}). \qquad (17)$$

TABLE 1 Reference values for the simulations

Model Parameter, Symbol	Reference Value
Cell radius, a	3.75 μm (Neelamegham et al., 1998)
Cell microvilli length, λ	0.4 μm (Shao et al., 1998)
Half chamber height, b	0.0127 cm
Length of flow chamber, L	2.0 cm
Inlet cell concentration, C_b	0.2×10^6 cells/ml
Fluid viscosity, μ	0.7 centipoise
Cell density, ρ_c	1.086 g/ml (Schneck, 2000)
Media density, ρ_m	1.0233 g/ml
Wall shear stress, τ_ω	2 dyn/cm^2
Rolling velocity, $u_r = \begin{cases} 2 \text{ dyn/cm}^2 \\ 0.5 \text{ dyn/cm}^2 \end{cases}$	4.0 μm/s 2.27 μm/s
Fraction of substrate area occupied at maximum cell density, f_{max}	0.025
Primary capture frequency, θ_{fr}	2/cm
Firm-arrest frequency, θ_{ra}	5/cm
Rolling-release frequency, θ_{rf}	0/cm
Adhesion-release frequency, θ_{ar}	0/s
Cell–cell capture probability, θ_{cc}	0

The concentration of rolling cells, C_r, in Region 4 is determined from the mass balance equation of this region,

$$\frac{\partial C_r^*}{\partial t^*} = -\frac{2bu_r}{\nu_{set}^{o} L}\frac{\partial C_r^*}{\partial x^*} + \frac{2b}{a}(R^* - R_{-1}^* - A^* + A_{-1}^*),$$

$$\begin{aligned} &\text{IC} \quad C_r^* = 0, \quad \text{at} \quad t^* = 0 \\ &\text{BC} \quad C_r^* = 0, \quad \text{at} \quad x^* = 0. \end{aligned} \tag{18}$$

where $A^* = A/C_b v_{set}^0$, $A_{-1}^* = A_{-1}^*/C_b v_{set}^0$, $C_r^* = C_r/aC_b$.

Model solution and usage

A finite difference scheme was used to determine the cell concentration in each of the $(m + m_1 + 3) \times n$ grid elements of the flow chamber. For this, the concentration in R1 was determined analytically from Eq. 8. Then the differential equations for the other regions (Eqs. 9, 14, 18) were converted from the 2D form (i.e., in the x and y direction) into a set of first-order differential-algebraic equations. During this transformation process, the equation corresponding to any point, say the ith element in the jth row of the 2D grid was translated into the $(j - 1)*n + i$th equation in the one-dimensional system of equations. The FORTRAN subroutine DDASPG in the IMSL library was then applied to solve the system of differential algebraic equations. The reference values for the parameters used in the simulations are given in Table 1. This corresponds to the case of neutrophil-like particles flowing and adhering on E-selectin and ICAM-1 bearing substrates. Whereas the first nine variables are determined from the physical parameters of the experimental system, the next two parameters (u_r and f_{max}) were determined directly from independent experiments that quantify cell-rolling velocity and maximum substrate occupancy. The final five variables are frequency and probability parameters that define the nature of the receptor–ligand interactions. These were obtained by fitting the experimental data.

To obtain estimates of θ_{fr}, θ_{rf}, θ_{ra}, θ_{ar}, and θ_{cc} for any experiment, the mathematical model was run for a range of frequency and probability parameters, and the output data was collected in terms of the number of rolling and adherent cell densities. Although a large number of combinations for the five parameters are possible, in most experimental situations, one or more of the frequency parameters can be set to zero. For example, in all our experiments, because we did not observe the release of either rolling or adherent cells back into the flow stream, θ_{rf} and θ_{ar} were set to zero. In some of the runs performed with DREG-56, which blocked secondary adhesion, we also set θ_{cc} to zero. Thus, by varying θ_{fr} and θ_{ra} in these simulations and upon comparing with the experimental data, we deduced the appropriate frequency- and probability-parameter values. Independent experiments and simulations were also performed in which we varied the inlet cell concentration in the flow chamber. Here, we confirmed that we could fit rolling and adhesion data over the range of inlet-cell concentrations with the identical frequency- and probability-parameter values at any given shear stress.

Estimating the intrinsic selectin on rate

Bonding between selectins and their ligands is facilitated by Van der Waal forces and electrostatic interactions, which eventually mediate the coordinated formation of a series of hydrogen bonds between the receptor and ligand (Graves et al., 1994). Formation of such interactions between a single receptor and ligand is termed a single bond. Currently, although it is thought that engagement of only a few neutrophil selectin–ligand bonds may be sufficient to initiate cell tethering and rolling over the range of physiologically relevant shear stresses, it is not established if a single selectin–ligand bond would be sufficient (Alon et al., 1995; Evans et al., 2001). In our analysis, we estimate the selectin on rate by defining a bond as the minimum set of hydrogen bonds that can mediate the tethering of cells. No assumption is made on whether this minimum set involves either single or multiple selectin molecules. We also assume that this tethering event only involves a single cell-surface microvillus because this is a likely scenario. In this regard, the selectins and their ligands are preferentially located on the neutrophil microvilli. Also, because our analysis is applied to analyze experiments with a high ligand density where rolling cells do not revert back into the free stream, we assumed that the formation of a single transient tether is sufficient to initiate stable cell rolling.

A previously published analysis method (Chang and Hammer, 1999) was adopted in conjunction with our estimates of primary capture frequency (θ_{fr}) to determine the selectin on rates from parallel-plate flow-chamber data.

First, the capture or tethering of cells from the free stream in region R3 by the ligand-bearing substrate is described by a first-order rate expression (Eq.19). Here, k_{ad} (unit of time^{-1}) is termed adhesion rate constant.

$$\frac{1}{a}\frac{dC_r}{dt} = k_{ad}C|_{y=R3}. \quad (19)$$

Thus, if $t_{1/2}$ denotes the time taken for the average cell in R3 to change from the free-stream to rolling, based on the above equation, $k_{ad} = \ln(2)/t_{1/2}$. In our analysis, we have shown above that $t_{1/2}$ is related to the primary capture frequency according to $t_{1/2} = \ln(2)/(u_f|_{y=R3}\theta_{fr})$. Therefore,

$$k_{ad} = u_f|_{y=R3}\theta_{fr}. \quad (20)$$

As discussed elsewhere (Chang and Hammer, 1999), the k_{ad} estimated above is a linear function of the number of cell-surface receptors in the cell–substrate contact region N_R and ligand concentration C_L (sites/area). Thus, these authors defined a forward rate constant k_f (unit of area/time) that is independent of the receptor and ligand number,

$$k_f = k_{ad}/(C_L N_R). \quad (21)$$

The forward rate constant k_f depends not only on the intrinsic reactivity between the receptor and ligand, but also on the rate at which the transient receptor–ligand complex forms. As the cell flows in the free stream in contact with the substrate, both the fluid convective flow and the receptor/ligand surface diffusivity contribute to the formation of this receptor–ligand complex. The rate of complex formation is thus dependent on the receptor/ligand diffusivity (D), the size of the encounter complex (a_e), and the relative convective velocity ($|\mathbf{V}|$) between the cell and the substrate. Because there is substantial slip near the flow-chamber substrate (Goldman et al., 1967), both the cell's free-stream velocity and rotation rate are accounted for while estimating the relative convective velocity, i.e., $|\mathbf{V}| = u_f - \Omega \cdot a$, where the angular velocity $\Omega = \gamma_w(1 - 5/16 \times (a/y)^3)/2$ (Goldman et al., 1967). Chang and Hammer solved the 2D convection–diffusion equation for cell interaction with the flow-chamber substrate. They introduced the Peclet number ($Pe = |\mathbf{V}|a_e/D$) to contrast the roles of diffusion and convection. In the context of selectin-mediated tethering and rolling where the radius of the selectin–ligand complex is 2.0×10^{-7} cm (Springer, 1990) and D is $\sim 10^{-10}$ cm^2/s (Chang and Hammer, 1999), Pe equals 10 at a wall shear rate (γ_w) of 28/s. Thus, typically, $Pe \gg 1$ in the flow chamber, i.e., it is cell convection rather than receptor diffusivity which controls the rate of selectin–ligand encounter complex formation. Under these conditions, Chang and Hammer showed by the theory of first passage (Szabo et al., 1980) that the duration of each encounter complex, t_e, is $8a_e/(3|\mathbf{V}|\pi)$. The binding probability, P, which is defined as the probability that the selectin has bound its ligand before the dissolution of the encounter complex, is then

$$P = k_f/(2DPe). \quad (22)$$

For a given value of the binding probability, P, and the duration of the encounter complex, t_e, we can then estimate the intrinsic on-rate k_{in} according to (Chang and Hammer, 1999)

$$k_{in} = \frac{P}{t_e(1-P)} = \frac{1}{t_e}\left[\frac{2|\mathbf{V}|a_e C_L N_R}{u_f|_{R3}\theta_{fr}} - 1\right]^{-1}. \quad (23)$$

In this analysis, the molecule on the cell surface is denoted as the "receptor" and the "ligand" is defined to be the surface-immobilized molecule. In the context of our flow-chamber experiments, it is not currently possible to estimate precisely a value for N_R (number of selectin ligands) because sufficient information on the nature of cell–substrate contact area at the instant when tethering occurs is not available. For this reason, we prefer to lump the intrinsic on-rate k_{in} and N_R into a lumped on rate denoted by k_{on},

$$k_{on} = k_{in}N_R \approx \frac{u_f|_{R3}\theta_{fr}}{2t_e|\mathbf{V}|a_e C_L}. \quad (24)$$

EXPERIMENTAL METHODS

Cell culture and neutrophil isolation

Fresh human blood was collected by venipuncture into a sterile syringe containing 10 U/ml heparin (Elkins-Sinn, Cherry Hill, NJ). Neutrophils were isolated using a one-step Ficoll-Hypaque gradient (ICN Biomedicals, Aurora, OH) as described previously (Taylor et al., 1996). Isolated cells were kept in Ca^{2+} free HEPES buffer (NaCl 6.428 g/l; KCl 0.746 g/l; $MgCl_2 \cdot 6H_2O$ 0.427 g/l; Glucose 1.8 g/l; HEPES 7.149 g/l) with 0.1% human serum albumin (Bayer Corporation, Elkhart, IN) at 4°C before the experiment. All reagents were from Sigma Chemical Co. (St. Louis, MO) unless otherwise mentioned.

Parent mouse fibroblast L cells (abbreviated L cells), and L cells transfected to either express ICAM-1 (I cells), or both ICAM-1 and E-selectin (E/I cells) were kindly provided by C.W. Smith (Baylor College of Medicine, Houston, TX). Cells were cultured as described elsewhere (Gopalan et al., 1997; Simon et al., 2000). For the adhesion assays, the mouse cells were detached from tissue culture flasks by adding sterile PBS containing 5 mM EDTA, and then plated onto 35-mm tissue culture-treated petri dishes (Corning Class Works, Corning, NY) at $2–3 \times 10^6$ cells/ml. Cells were grown for 2–3 days till confluence before the experiment.

Cell adhesion experiments

Neutrophil adhesion experiments were performed in a parallel-plate flow chamber (Glycotech, Rockville, MD) mounted on the stage of a phase-contrast optical microscope (CK40, Olympus, Japan) with a 10× objective. All runs were performed at 37°C. A syringe pump (Kd Scientific, New Hope, PA) was used to simulate a uniform laminar flow field in the flow chamber. Here, the petri dishes with the confluent E/I cell monolayers were used as the ligand-binding substrate. The monolayer was perfused with sterile PBS for 4–5 min before introduction of the isolated neutrophil suspension, resuspended in HEPES buffer with 1.5 mM $CaCl_2$, at a predetermined concentration. In some experiments, where antibodies were used to block secondary tethering, neutrophils were preincubated with 15

μg/ml L-selectin antibody DREG-56 (purified from ATCC hybridoma culture supernatant) for 10 min before the start of the experiment. Independent experiments performed in a neutrophil homotypic aggregation assay confirmed that DREG-56 blocks ~100% of the L-selectin interactions between neutrophils (data not shown). In our runs, the cell-rolling and adhesion data were recorded using a CCD camera (Model 77, MTI-Dage, Michigan City, IN) and time-lapse video recorder (TLC2100, GYYR, Anaheim, CA). During the first 9 min of each experiment, data was recorded at a fixed position of the flow chamber. Following this, the field of observation was moved to 5 other random locations and cell binding data was recorded at each position for 20s. Data analysis was performed after completion of the entire experiment by digitizing the images using a Scion LG3 board (Scion Corp., Frederick, MD) and using PC-based NIH-Image software (Scion).

In other experiments, performed with a chimeric E-selectin fusion protein (Glycotech, Rockville, MD), which consisted of the E-selectin extracellular domain fused to an IgG tail, we examined whether E-selectin was a prominent ligand for L-selectin on neutrophils. In these runs, we observed that the binding of the E-selectin fusion protein to isolated human neutrophils could not be blocked by an antibody against the lectin domain of L-selectin (DREG-56). However, this interaction could be blocked by anti-human E-selectin monoclonal antibody HAE-1f (Ancell, Bayport, MN). This suggests that E-selectin does not bind the neutrophil L-selectin lectin domain. This domain is thought to contribute to neutrophil tethering.

E-selectin density on cotransfected cells

The E-selectin site density on cotransfected cells was determined using the Quantum Simply Cellular microbead standards (Bangs Laboratories, Fishers, IN) in conjunction with mouse anti-human E-selectin antibody, CL2/6 (Biosource International, Camarillo, CA). These uniform microbeads have a calibrated number of goat-anti-mouse IgG sites on their surface. In these runs, both the calibrated microbeads and the cotransfected E/I cells were incubated with CL2/6 at saturating concentrations. After a brief wash in HEPES buffer, a secondary Alexa-488 conjugated $F(ab')_2$ goat anti-mouse IgG (H + L) antibody (Molecular Probes, Eugene, OR) was added for 10 min. The beads and cells were again washed rapidly and the samples were read using a flow cytometer. The number of E-selectin sites per E/I cell was then determined by quantifying the fluorescence intensity of the labeled cells, and translating this value to the number of bound antibodies using the microbead standards. Isotype matched controls were also performed to confirm the findings.

Data analysis

The number of rolling cells and adherent cells was determined at each time point. For these measurements, the density of adherent cells was determined at each time point by counting the number of cells that moved by less than 1 cell diameter in a given 20-s time period. The number of rolling cells was then estimated by subtracting the number of firmly adherent cells from the total number of cells.

In some runs, the rolling velocity of neutrophils was also determined by randomly choosing 40–50 rolling cells and following their motion for ~20 s. Rolling velocity was determined by dividing the distance traveled by these cells by the time taken. ANOVA analysis using the Student Newmann Keul's test was performed to assess statistical differences between experimental runs. $p < 0.05$ was considered significant.

RESULTS

The mathematical model for cellular interactions in the parallel plate flow chamber was simulated over a range of conditions that are typical for biological experiments. A summary of the results is presented here. In addition, the model was fit to experiments that elaborate on the nature of selectin- and integrin-mediated adhesion. All reference parameters for the simulations are listed in Table 1, unless otherwise stated. These correspond to the case of isolated human neutrophils rolling on E/I cells.

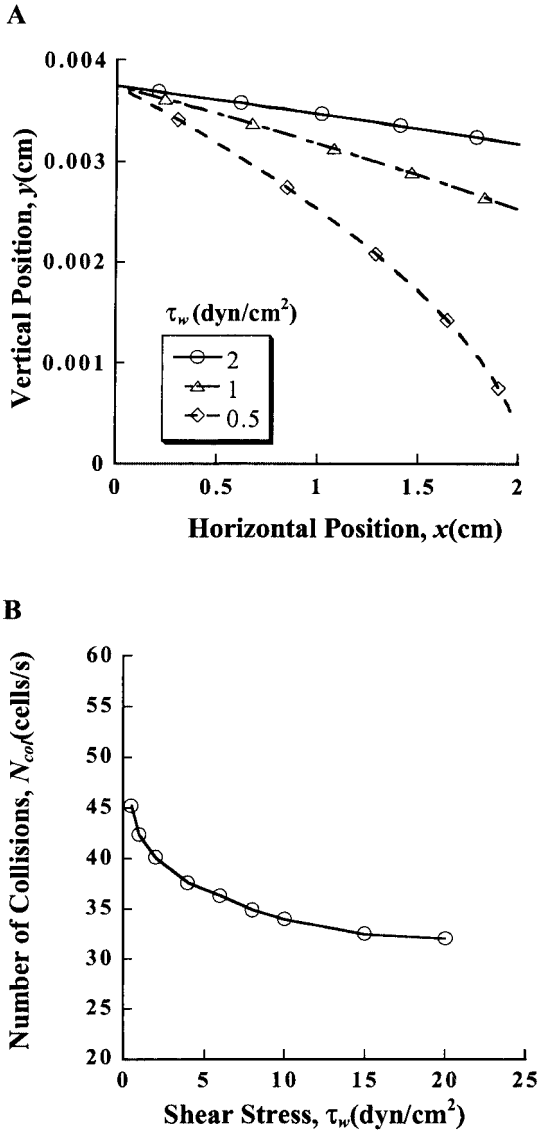

FIGURE 3 Cell trajectory in flow chamber. (*A*) Trajectories of cells entering the flow chamber at a height of ten cell radii i.e., $(x_0, y_0) = (0, 10a)$. Wall shear stress varies from 0.5 to 2 dyn/cm^2. All other parameter values are given in Table 1. In typical experiments, a majority of cells introduced into the flow chamber do not collide with the substrate. (*B*) Total number of cell–substrate collisions decreases with increasing shear.

The rate of cell–substrate collision depends on fluid convection and cell settling velocity

Figure 3 *A* presents the trajectory of cells in the flow chamber during typical biological studies. For these calculations,

although particle convective velocity far above the substrate was assumed to follow a parabolic profile (Eq. 3a), it was estimated using Goldman's equation (Eq. 3b) near the substrate. The settling velocity near the substrate is also lower than free settling velocity due to the presence of lubrication layer (Eq. 2). For the flow chamber geometry considered, above a shear stress of 0.5 dyn/cm^2, cells that enter the flow chamber at a height above the ten-cell radius mark (i.e., $y_0 > 10a$) do not contact with the plate surface. Thus, typically, a majority of the cells introduced into the flow chamber do not contribute to cell rolling or adhesion.

We examined whether the number of cells contacting the substrate per unit time, N_{col}, (Eq. 5) is a function of the applied shear stress (Fig. 3 *B*). Two competing features regulate this parameter: although increasing the shear stress increases the number of cells entering the chamber per unit time, the higher convective velocities simultaneously reduce the time available for cell settling onto the substrate. As seen in Fig. 3 *B*, N_{col} decreases by ~25% on increasing the applied shear stress from 0.5 to 20 dyn/cm^2. In general, at 2 dyn/cm^2, for the range of flow chamber sizes considered (L varied from 0.5 to 4 cm, and b from 0.0127 to 0.0254 cm), we observed that the percentage change in N_{col} with shear rate is independent of the flow chamber geometry. It is primarily regulated by the physical properties of the cells (density and size), the properties of the liquid (viscosity and density) and the applied shear rate.

Cell concentration near the plate surface may be higher than inlet cell concentration

Accurate estimation of the cell concentration close to the substrate is important because the density of rolling and adherent cells is a strong function of this parameter. For this reason, we compared the cell concentration: far from the substrate (in R2a at $y \geq 4a + \lambda$); near the substrate (in R2b, $4a + \lambda > y \geq a + \lambda$); and in region R3 ($a + \lambda > y \geq a$) where the cell microvilli are in contact with the substrate.

We observed that, away from the substrate in R2a, the steady-state cell concentration is independent of the nature of cell rolling and adhesion, quantitatively equal to the inlet cell concentration, and independent of the distance from the chamber entrance (data not shown). Further, the upper wall of the flow chamber does not affect the manner of cell settling near the ligand-coated substrate.

Near the substrate in R2b, however, we observed that the cell concentration was higher than the inlet concentration, C_b (Fig. 4, *A* and *B*). In this region, steady-state cell concentration was achieved rapidly, typically in less than 10s. (Fig. 4 *A*). The time taken was approximately equal to the time taken for the cells to convect from the entrance of the flow chamber to that region. The steady-state concentration at the bottom of R2 increased with proximity to the substrate (Fig. 4 *B*). This is apparently because of the effect of the lubrication layer near the substrate, which reduces the cell settling velocity and consequently increases the accumulation near the substrate. In support of this proposition, we observed that, upon neglecting the lubrication effects (i.e., assuming that v_{set} was equal to the free settling velocity v^o_{set} independent of position in the flow chamber), the predicted cell concentration was uniform and equal to C_b in all sections of R2 (data not shown). The lubrication layer also causes positional variations in the cell concentration at the bottom of R2 with distance from the flow chamber entrance. We observed, using our default simulation parameters (Table 1), that, although the concentration near the entrance equals the inlet concentration C_b, it increases with distance from the entrance (data not shown). This lubrication feature may thus contribute to the variation in cell concentration with position in the flow chamber.

Finally, we considered the cell concentration in R3 (Fig. 4 *C*). The concentration of cells in this region is not only dependent on the rate of settling and convection, it is also influenced by the rate of cell tethering onto the flow chamber (Eq. 14). If the rate of cell tethering is lower (i.e., θ_{fr} is small) than the flux of cells into this region, then there is net accumulation of cells in this region. This results in an increase in cell concentration with distance from the flow chamber inlet (Fig. 4 *C*, $\theta_{fr} = 2$/cm). In the converse case, if the rate of cell tethering is larger ($\theta_{fr} = 20$/cm), positional variations may be less prominent. Overall, the hindered settling of cells onto the flow chamber substrate causes positional variations in the cell concentration near the substrate, and it necessitates the complete solution of cell concentration in all regions of the flow chamber.

Conversion of rolling and adherent cell density into adhesion frequency parameters

In typical flow chamber runs, the measured parameters in experiments are rolling cell density and adherent cell density. These parameters are functions of both the physical features of the system that influence the rate of cell–substrate and cell–cell collision and the biological features that influence the cellular adhesivity. Our model attempts to quantify the contribution of the biological adhesivity of cells independent of the physical parameters. To achieve this, we introduce various adhesion frequency and probability parameters. Figure 5, *A* and *B*, depict contour plots for cell rolling and adhesion density, respectively, for a range of primary capture (θ_{fr}) and firm-arrest frequencies (θ_{ra}) at 10 min for a wall shear stress of 2 dyn/cm^2 near the center of the flow chamber ($x^* = 0.4$). For the sake of simplicity, in these simulations, all other frequency parameters that contribute to cell–cell interactions (θ_{cc}) and the release of cells from the substrate (θ_{rf} and θ_{ar}) are set to zero. Here, the cells in region R4 are defined to be rolling, and the accumulation of cells in this region is a measure of the rolling cell density (Eq. 18). The number of cells exiting R4 via adhesive interactions was used to quantify the adherent cell density

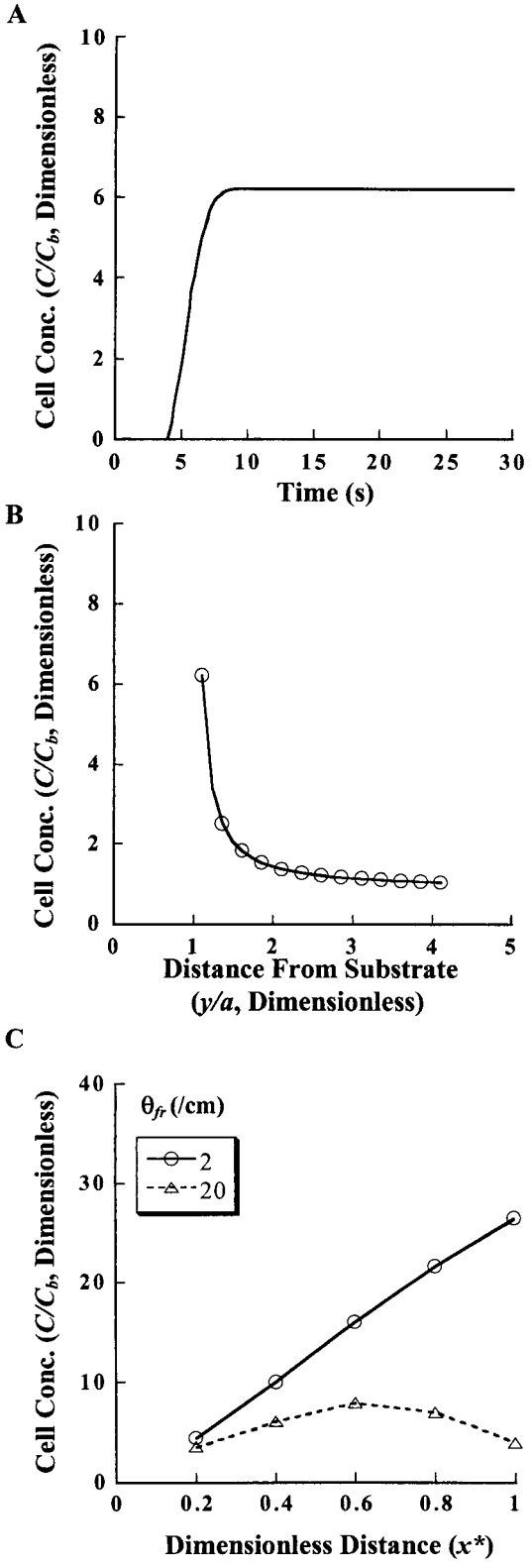

FIGURE 4 Cell concentrations near the plate surface. (*A*) Temporal evolution of cell concentration in the last row of R2b at dimensionless position $x^* = 0.4$. Steady state is achieved within seconds and the final cell concentration in this region is ~6 times inlet cell concentration. (*B*) Steady-state cell concentration in R2b increases dramatically with proximity to the flow chamber substrate. Data are presented for dimensionless position $x^* = 0.4$. (*C*) Positional variation in cell concentration in R3 at 10 min. The concentration of cells may either decrease or increase with distance from the flow chamber entrance depending on the relative magnitude of the cell settling velocity and primary capture frequency. All simulation parameters, except θ_{fr} in (*C*), are given in Table 1.

(Eq. 17). Because cell capture and adhesion are sequential events, increasing the capture frequency augments both the cell rolling and adhesion densities (Fig. 5). Similarly, increasing adhesion frequency both increases the number of adherent cells and decreases rolling cell density. Overall, for given experimental data that quantifies cell rolling and adhesion density, contour plots such as those in Fig. 5 can be used to convert data on cell rolling and adhesion density into adhesion frequencies.

Time to achieve steady rolling density is inversely proportional to cell rolling velocity

Experiments were performed to examine the ability of the model to fit real data. In these runs, neutrophils tethered, rolled, and arrested on mouse fibroblasts bearing human E-selectin and ICAM-1. In this system, neutrophils tether onto substrates via E-selectin (Gopalan et al., 1997). Engagement of E-selectin causes signaling via the mitogen-activated protein kinase (MAPk) signal transduction pathway and activation of the β_2-integrin (Simon et al., 2000). The activated β_2-integrins then bind both ICAM-1 and other unidentified ligand(s) on the cotransfectants. This results in the firm arrest of neutrophils onto the substrate. In control experiments, we verified the role of E-selectin and β_2-integrins in tethering, rolling, and firm adhesion (data not shown). Also, neutrophils do not roll on or adhere to either parent L-cells, or L-cells transfected with ICAM-1 alone. Overall, in this system, tethering is E-selectin-mediated and firm arrest takes place via the β_2-integrins.

The first set of experiments (Fig. 6) was performed in the presence of 15 μg/ml anti-L-selectin-blocking antibody DREG-56 to prevent secondary tethering. The inlet cell concentration was held constant at 0.2×10^6 cells/ml while the applied shear stress was varied from 0.5 to 4 dyn/cm^2 (Data for 2 dyn/cm^2 is presented in Fig. 6 *A*). Several observations were made: 1) Over the 10-min duration of the experiment, the rolling cell density increased with time and did not quite achieve steady state. This is in contrast to the cell concentration just above the substrate in R3 where steady state was achieved within 10 s (Fig. 4 *C*). Simulations were performed to examine the parameters controlling the cell rolling density. For these calculations the primary capture frequency and rolling velocity were varied while the firm-arrest frequency was kept constant. The calculations revealed that, although the magnitude of the cell rolling density is a strong function of the primary capture frequency, the time to reach maximum rolling density is pri-

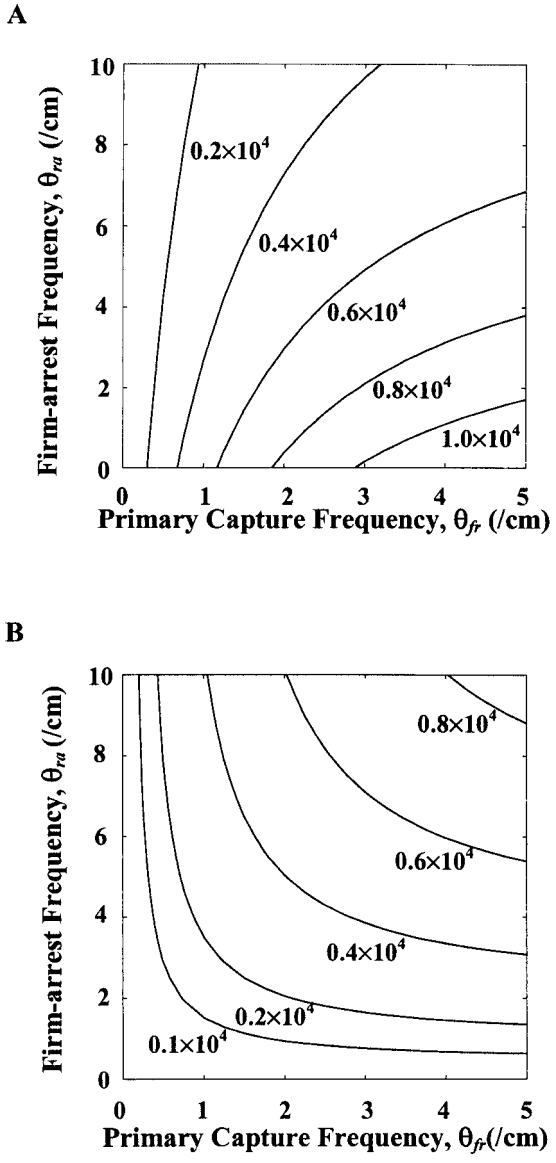

FIGURE 5 Model predictions of rolling and adhesion cell density contours depict lines of (*A*) equal rolling cell density and (*B*) adherent cell density. Values of either rolling or adherent cell density (in cell/cm^2) are provided next to each contour line. The dependence of these parameters on primary capture frequency (θ_{fr}) and firm-arrest frequency (θ_{ra}) is shown at $\tau_\omega = 2$ dyn/cm^2, $t = 10$ min and $x^* = 0.4$. Values of all other parameters are listed in Table 1.

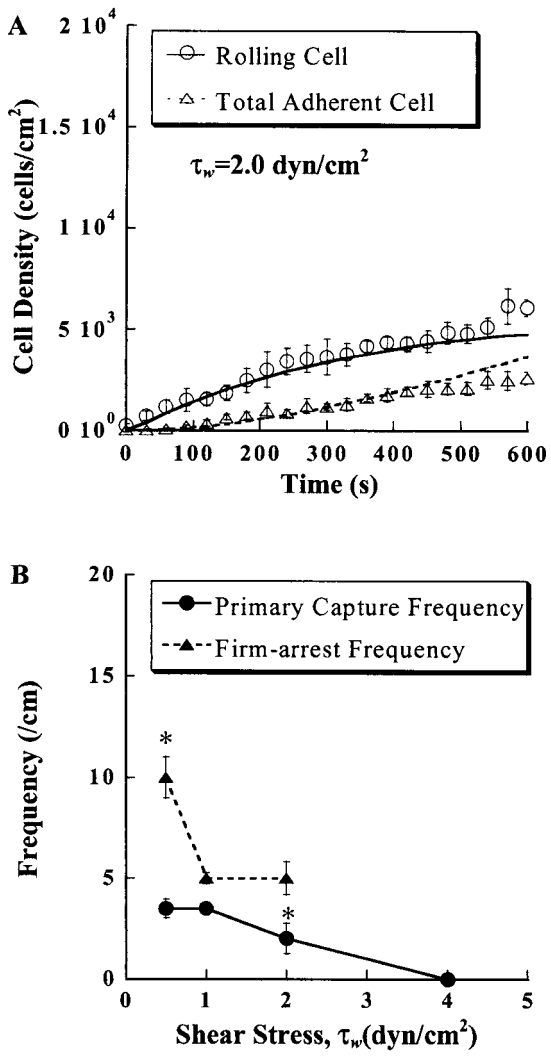

FIGURE 6 Model estimate of primary capture and firm-arrest frequency over a range of shear stresses. Rolling cell density and adherent cell density were measured in experiments when 0.2×10^6 neutrophils/ml were passed over E/I cells over a range of shear stresses (0.5–4 dyn/cm^2). In all these runs, neutrophils were preincubated with 15 μg/ml DREG-56 to prevent secondary tethering. (*A*) Comparison of experimental data (*discrete points*) and model fit (*smooth lines*) is presented at $x^* = 0.4$ for a wall shear stress of 2 dyn/cm^2. Data for other shear conditions are not shown. (*B*) Primary capture and firm-arrest frequency obtained by modeling data over the range of shear stresses. Error bars are mean ± SEM for $N \geq 3$. * $p < 0.05$ with respect to all other shear stresses.

marily dependent on cell rolling velocity. This time is insensitive to the value of primary capture frequency. Overall, the distinct time-scales required to achieve either steady free-stream concentration or constant cell rolling density is due to the large difference between the cell free stream velocity and rolling velocity. Thus, at a shear rate of 2 dyn/cm^2, because the free stream velocity near substrate (739 μm/s) is ~180 times greater than the rolling velocity (4.0 μm/s), it may be expected that the time to achieve steady state is also ~180 times larger. 2) Although the number of rolling cells increased rapidly in the first few minutes, this rate of cell accumulation slowed down at the later time points. This was apparently due to a decrease in the substrate area available for cell recruitment as predicted by Eq. 12. 3) The model estimates that, at 2 dyn/cm^2, 28% of the cells that collided with the substrate changed to rolling by primary capture mechanism. This percentage increased to 34% at 0.5 dyn/cm^2 (data not shown). 4) Over the range of experimental conditions, adherent cells accounted for ~20% of all surface-bounds cells. Also, the

TABLE 2 Average time $t_{1/2}$

Shear stress (dyn/cm^2)	0.5	1	2
Time for change from free stream to rolling (s)	8.73 ± 1.06	3.96 ± 0.31	3.24 ± 0.93
Time for change from rolling to firm-arrest (s)	293.54 ± 22.75	473.85 ± 25.67	362.01 ± 63.68

adhesion flux, A, was approximately proportional to the rolling cell density as proposed in Eq. 15.

Contact duration required for neutrophil tethering onto E-selectin is ~4–8.5s

The experimental data discussed above, over the range of shear stresses, were fit to the mathematical model by varying two frequency parameters, the primary capture frequency (θ_{fr}) and the firm-arrest frequency (θ_{ra}). θ_{cc} was set to zero because all secondary capture is blocked in these runs. θ_{rf} and θ_{ar} were also zero because the reversible release of rolling or adherent cells from the substrate was not observed. In the modeling results summarized in Fig. 6 *B*, it is apparent that the capture frequency decreased significantly with increasing shear stress. For the entire range of shear tested the time taken for cell capture ($t_{1/2} = \ln(2)/(\theta_{fr}u|_{R3})$) was in the order of ~4–8.5 s (Table 2). Similar to the observations for primary capture, we also observed that the distance that the cell rolled before changing to firm arrest also increased with shear stress. The time required for firm arrest ($t = \ln(2)/(\theta_{ra}u_r)$) was ~300 s independent of the applied shear (Table 2). Thus, the rolling neutrophil samples the L-cells for a critical amount of time before β_2-integrin activation and firm arrest.

Secondary capture is significant at higher cell concentrations

To examine the contribution of secondary attachment in flow chamber experiments, runs were performed in the absence of the L-selectin-blocking antibody over a range of inlet cell concentrations from 0.1×10^6 to 0.5×10^6 cells/ml (Fig. 7) and shear stresses (data not shown). Over the range of conditions, we observed that the number of rolling and adherent cells was ~1.5-fold higher in the absence of the anti-L-selectin-blocking antibody as compared to the runs with the antibody (Fig. 7, data not shown). Secondary tethering caused cell rolling in clustered patches in the absence of the L-selectin antibody. In contrast to this, on addition of DREG-56, the rolling cells were distributed approximately uniformly on the chamber substrate. Finally, secondary tethering contributed more markedly to rolling and adherent cell density at the higher inlet cell concentrations. This is apparently because increasing the inlet cell concentration increases both the free stream cell concentration and the rolling cell density. These two parameters are directly related to the secondary capture flux, R_s (Eq. 11).

Experimental data over the range of inlet cell concentrations were fitted with the mathematical model (Fig. 7). These runs were performed at a constant shear stress of 2 dyn/cm^2. The primary capture frequency and the firm-arrest frequency used for the model fit were obtained from the runs with the anti-L-selectin antibody, i.e., $\theta_{fr} = 2$/cm, $\theta_{ra} = 5$/cm (Fig. 6 *A*). The secondary capture probability was then set to $\theta_{cc} = 0.07$ and the entire dataset over the range of cell concentrations were fit (Fig. 7, *A–C*). Similar data fits were performed at lower shear rates, and they revealed that the secondary capture probability was higher at the lower shears ($\theta_{cc} = 0.2$). This suggests that, in typical experiments ~7–20% of the collisions between cells in the suspension and surface-bound cells may result in secondary capture. The ability of our model to fit data over a range of cell concentrations and shear rates provides partial validation of the model.

Estimating the on-rates of the selectins

We compared the E-selectin on-rates obtained from our neutrophil-E/I cotransfectant experiments (Fig. 6) with that of other runs, where neutrophils bound reconstituted substrates composed of immobilized soluble E-selectin (Puri et al., 1997). First, we converted the experimental data in the two systems to obtain the primary capture frequency, $\theta_{fr,}$ as a function of shear stress (Fig. 8 *A*). θ_{fr} for our experimental data with cotransfectants was estimated in Fig. 6. For the experiments in the reconstituted system, the experimental data on primary tethering flux R_P provided by (Puri et al., 1997) was used to estimate θ_{fr} by applying our mathematical model. The E-selectin density on the substrate (C_L) for the reconstituted systems is known (Puri et al., 1997), and, in our system, we estimated this to be ~121 receptors/μm^2 using the microbead standards as described in Methods. As seen in Fig. 8 *A*, the primary capture frequency decreases with shear rate for both the experimental systems. Thus, at the higher shear rate, the cell travels a larger distance in region R3 before tethering. We estimated the time spent by the cells in the free stream in region R3 before primary capture (i.e., $t_{1/2} = \ln(2)/(\theta_{fr}u_f)$). For any given receptor density this time spent in R3 did not vary markedly with shear stress, suggesting that neutrophil tethering onto the E-selectin substrate is a contact-duration-dependent process. This time also decreased approximately linearly with increasing ligand density from ~16.5 s at $C_L = 55$, to 6.0 s at $C_L = 80$ down to 2.73 s at $C_L = 180$.

Data on primary capture frequency, $\theta_{fr,}$ was converted to estimate the lumped on-rates using Eq. 24 (Fig. 8 *B*). As seen, the E-selectin lumped on-rates, k_{on}, lies in the order of 100–300/s over the entire range of shear stress from 0.84–3

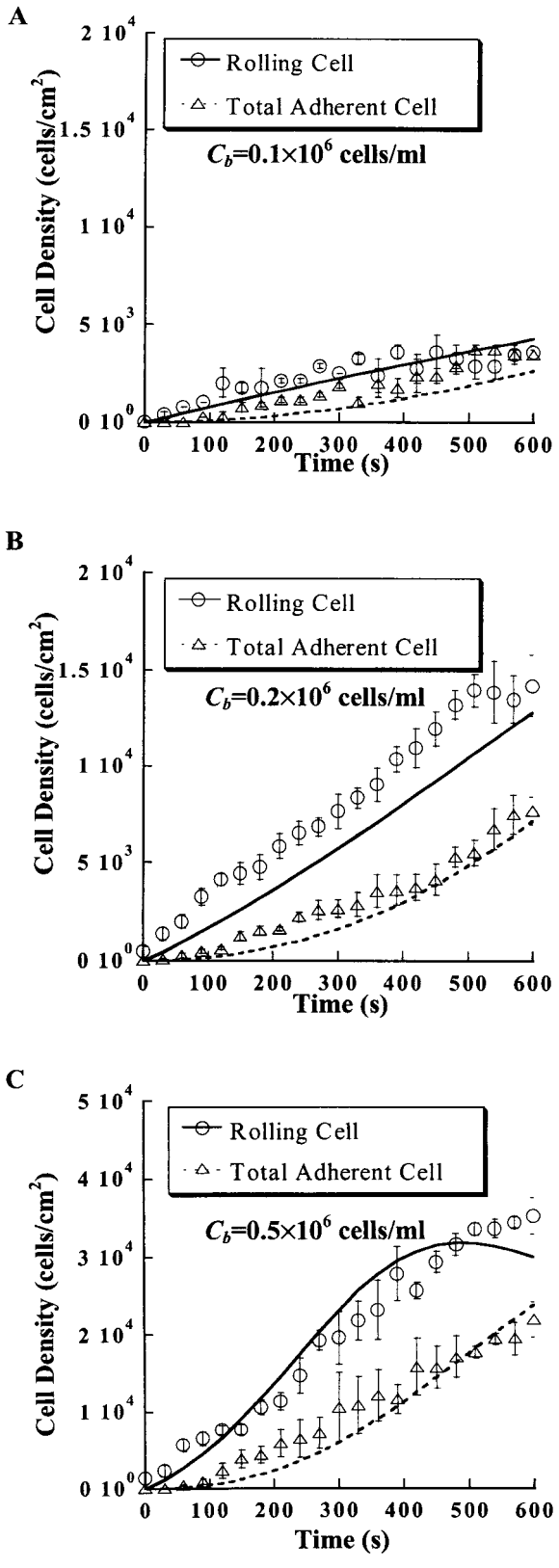

FIGURE 7 Secondary tethering at high inlet cell concentration. Neutrophils over a range of cell concentrations from 0.1 to 0.5 × 10^6 cells/ml were introduced into the flow chamber at τ_ω = 2 dyn/cm^2 in the absence of anti-L-selectin-blocking antibody. Tethering to E/I cells was possible via both primary and secondary capture mechanisms. Data for the following inlet cell concentrations are presented at position x^* = 0.4 in the flow chamber: (*A*) 0.1 × 10^6 cells/ml, (*B*) 0.2 × 10^6 cells/ml, and (*C*) 0.5 × 10^6 cells/ml. The rolling and adherent cell density were calculated over the time course of the experiment (*discrete points*) and compared with simulation results (*smooth lines*). The model parameters, θ_{fr} = 2/cm, θ_{ra} = 5/cm, and θ_{cc} = 0.07, were applied to fit experimental data in (*A*)–(*C*). Note that the θ_{fr} and θ_{ra} values are the same as in Fig. 6. All other parameters are listed in Table 1. Error bars are mean ± SEM for $N \geq 3$.

dyn/cm^2. Several observations were made during this analysis: 1) The selectin on-rate estimated from both the reconstituted and cellular systems were of comparable magnitudes, and they did not vary markedly with shear stress. 2) The estimated on-rate in the reconstituted system at 80 and 180 sites/μm^2 were independent of the receptor number. This reflects the fact that the estimated on-rate is a function of the biological properties of individual bonds and it is not a function of receptor density.

Similar calculations were performed with additional data provided by Puri et al. for P- and L-selectin at shear stresses ranging from 0.84–3 dyn/cm^2 when the receptor density was 90 selectins/μm^2. Here, we observed that the lumped on-rates of the three selectins varied as: L-selectin (1000/s) > P-selectin 300–450/s) > E-selectin (100–250/s).

DISCUSSION

Estimation of "adhesion efficiency" in the parallel-plate flow chamber

We developed a mathematical model to interpret cell adhesion data obtained from a parallel-plate flow chamber under dynamic flow conditions. Although conventional analysis techniques quantify cell adhesion rates by measuring the density of rolling and adherent cells with time, we propose an alternate strategy. This involves quantification of the various types of cellular interactions based on a series of frequency and probability parameters. We propose that this strategy allows us to better distinguish between the effects of the physical features of the flow system that influence cell–cell and cell–substrate collision frequency, and the biological features that are a measure of cellular adhesivity. Further, the analysis strategy allows us to delineate between the contributions of adhesion molecules in mediating primary and secondary capture in the flow chamber. We note that similar strategies have been previously developed to examine cell–cell adhesion in suspension (Bell et al., 1989; Neelamegham et al., 1997b) and homotypic cell aggregation on substrates (Neelamegham et al., 1997a). Strategies to decouple transport and reaction features have also been developed for other experimental systems (Myszka et al., 1998).

In this paper, we test our model with a series of experiments where neutrophils bind to E/I cells in an in vitro model of inflammation. In these runs, the experimental data

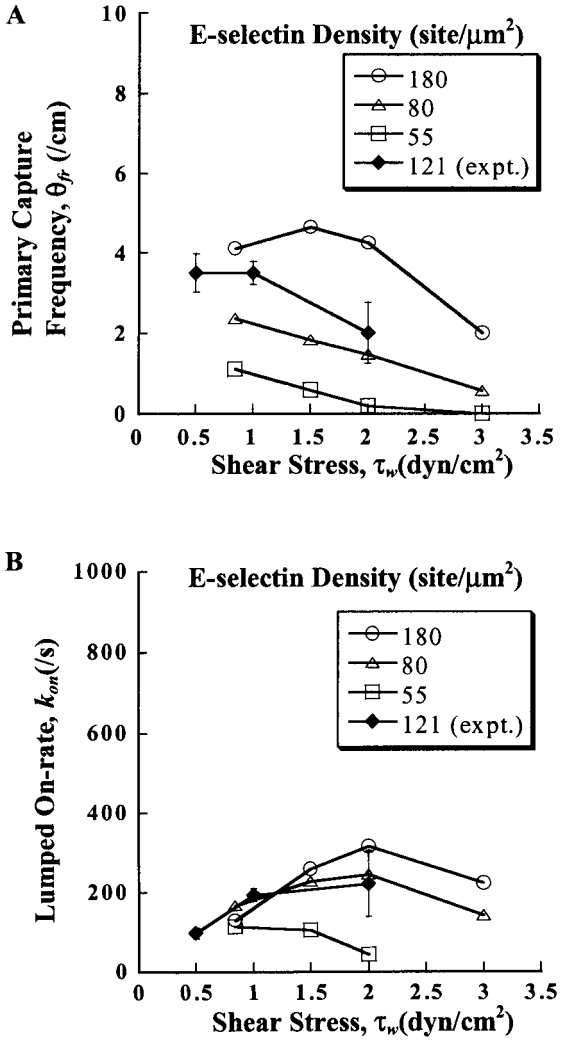

FIGURE 8 Primary capture frequency and E-selectin on-rates. Data for E-selectin binding kinetics from our experimental system (E-selectin density = 121 sites/μm^2) were compared with data from a reconstituted system where neutrophils bound soluble E-selectin coated substrates (E-selectin density = 55, 80, or 180 sites/μm^2). (*A*) The data in both cellular and reconstituted systems was used to estimate the primary capture frequency, θ_{fr}. θ_{fr} decreases with shear and increases with receptor density. (*B*) The lumped on-rate was then estimated over the range of experimental conditions. The on-rate is only a weak function of the applied shear rate and E-selectin site density (except for 55 sites/μm^2). Error bars are mean ± SEM for $N \geq 3$.

was modeled over a range of conditions including inlet cell concentrations, shear stresses and antibody treatments. Our ability to fit the data over a range of experimental conditions provides partial validation of the analysis strategy.

An interplay between the physical and biological features control cell rolling and adhesion rates

The application of the model revealed how the physical features of the system and the binding properties of the adhesion molecules may control positional variations in cell concentration within the flow chamber. In this regard, we observed that the reduction in cell settling velocity near the flow chamber substrate due to lubrication effects caused greater accumulation of cells near the substrate in comparison to the inlet cell concentration. This feature also caused variations in cell concentration in region R3 with distance from the flow chamber entrance.

The physical parameters in the system (Table 1) especially the cell and media density play a prominent role in controlling the rate of cell–substrate collision and rolling density. For example, our flow chamber simulations predict that, at the 10-min time point, the density of rolling neutrophils (ρ_c = 1.086 g/cm^3) would be twice that of rolling lymphocytes (ρ_c = 1.063 g/cm^3) provided the values of all other simulation parameters are identical to Table 1. Accounting for cell density during data analysis may thus be important in studies that contrast the affinity/avidity of cell adhesion molecules between different cell types (Patel and McEver, 1997).

A balance among the rate of cell settling, convection, and capture frequencies controlled the density of rolling cells. Thus, despite marked positional variations in cell concentration in R3, our simulations predicted only a moderate change in rolling cell density with position. Typically, in both the experiments and the simulations, we only observed an ~20% increase in cell concentration between the center of the flow chamber and the exit (data not shown). Although there is little variation in cell rolling density with position under our experimental conditions, the model predicts that such variations may be more pronounced in systems with a lower primary capture frequency.

The time taken for a system to reach steady state is dependent on the chamber size, shear rate, and cell rolling velocity. Our model suggests that the time scale required to achieve steady free-stream concentrations is dependent on the free-stream velocity at that point and the distance from the flow chamber inlet. Similarly, the time to achieve steady rolling density is directly related to the cell rolling velocity. Because the cell convection velocity is at least one order of magnitude greater than the rolling velocity in typical runs, steady cell densities will be more quickly achieved in the free-stream in comparison to the flow chamber substrate. Typically, experimental systems with smaller flow chambers, higher shear rates, and larger rolling velocities will require less time to achieve steady state. Thus, steady cell rolling density may be achieved more rapidly in experiments where soluble adhesion molecules are coated only in a small region at the center of the flow chamber.

Nature of cell–cell interactions in the flow chamber

In the vasculature, the secondary capture of cells by other rolling cells is thought to contribute to leukocyte recruit-

ment under specific shear conditions (Eriksson et al., 2001). Such phenomena has also been observed in flow chamber runs (Alon et al., 1995; Walcheck et al., 1996). In all these cases, neutrophil–neutrophil adhesive interactions are mediated by L-selectin and β_2-integrins (Simon et al., 1992; Taylor et al., 1996). The primary ligand for L-selectin is P-selectin glycoprotein ligand-1, PSGL-1 (Guyer et al., 1996). In our studies, we report that 7% of collisions between cells in suspension and surface-bound cells result in secondary capture at 2 dyn/cm^2 ($\gamma_w \sim 285$/s). The percentage of collisions resulting in secondary capture increased to $\sim$20% at 0.5 dyn/cm^2 ($\gamma_w \sim 71$/s). Although the secondary capture probability (θ_{cc}) estimated in this study cannot be directly compared with the efficiency of neutrophil homotypic adhesion measured in a cone-plate viscometer (Neelamegham et al., 1997b; Shankaran and Neelamegham, 2001), we note that the estimates of θ_{cc} at 71–285/s compare reasonably well with the efficiency of neutrophil–neutrophil binding in the viscometer at the same shear rate. The adhesion efficiency in the latter case was $\sim$0.1 at a shear rate of 100/s.

Besides providing an adhesive surface for secondary cell capture, surface-bound cells may also promote or inhibit cell tethering by altering the local hydrodynamic environment. In the Appendix, we present a simple analytical solution for the flow around a stationary sphere. Here, we report that adherent cells may alter the local fluid velocity up to 2.5 cell diameters away, along both the length and the height of the flow chamber. The disturbance to flow is equally prominent both upstream and downstream of the substrate-bound cell, and its magnitude is independent of the applied shear stress (Fig. A1 *B*). Thus, although cell–surface adhesion molecules mediate secondary capture, the local hydrodynamic environment may also influence the rate of cell recruitment. We speculate that, although the substrate-bound cells may reduce the local shear rate and promote tethering at low rolling densities, under conditions of higher substrate occupancy, these cells may limit additional recruitment of cells.

We note that it has been recently reported that carbohydrate-coated spherical beads tend to attach to the adhesive walls 4–5 cell diameters up- or downstream of a slowly rolling or stationary adhesive bead (King and Hammer, 2001). In that work, the authors perform a numerical analysis of two-body hydrodynamic interactions using adhesive dynamic simulations. The reason for the difference in our prediction that a bound cell only causes a disturbance to flow within 2.5 cell diameters, and the prediction of these authors that flow may alter cell binding up to 4–5 cell diameters is not clear. Perhaps, this is a feature of the manner in which the problems are treated.

In an independent set of experiments, we examined whether nonadhesive collisions between cells in suspension and other substrate-bound leukocytes may alter the rate of primary cell capture (Supplemental Material, www.eng.buffalo.edu/~neel/pplate.html). One mechanism contributing to this feature may involve the stabilization or destabilization of adhesive interactions between transiently tethered cells and the substrate. This may either promote or diminish the number of rolling cells. Alternatively, mechanical forces applied by cells in suspension on the substrate-bound rolling cells may either augment or reduce the latter's rolling velocity. In these experiments, performed with varying combinations of live neutrophils and fixed nonadhesive cells, we observed that nonadhesive interactions between the two cell populations did not affect the tethering flux or cell rolling velocity (Supplemental Material, www.eng.buffalo.edu/~neel/pplate.html).

The nature of selectin-and integrin-mediated adhesion

A key feature of the model is the ability to convert data on rolling and adherent cell density into primary capture (θ_{fr}) and firm-arrest (θ_{ra}) frequency. These frequency parameters are inversely related to the distance that the average cell travels either in contact with the flow chamber before changing to rolling, or in rolling motion before firm arrest. In the multistep paradigm of neutrophil rolling and arrest on the inflamed endothelium, the first parameter is related to the features that control selectin engagement and the latter parameter is related to the time taken for integrin activation and binding.

In our experiments, for the range of shear conditions, we observed that E-selectin had θ_{fr} values that were less than 4/cm. Thus, we estimated that, in typical experiments, the neutrophils flow in the flow stream in contact with the E-selectin substrate for $\sim$4–8.5 s before primary capture. To the best of our knowledge, this is the first such estimate of the time required for selectin engagement. Our observation that the time for E-selectin binding is relatively independent of the applied shear rate suggests that E-selectin-mediated binding may be contact duration dependent.

The primary capture-frequency parameter is a function of two features: the receptor density and the applied shear rate. As seen in Fig. 8, although the capture frequency increased with receptor density, it decreased with applied shear. In these experiments, the shear rate has two opposite effects: although it increases the rate at which receptor–ligand encounter complexes were formed, it simultaneously decreases the encounter duration of the selectin–ligand complex. With the objective of estimating a parameter that is independent of the rate and duration of receptor–ligand encounter complex formation, we estimated the lumped on-rate, k_{on} (Eq. 24) based on work by Chang and Hammer (1999). Here, we observed that: 1) The esti-

mated on-rate for data in the reconstituted systems matched closely with our data in a cellular system. 2) Both systems appeared to scale well with applied shear stress and receptor number because the lumped on-rate is only a weak function of these parameters. A notable exception to this was data at the lowest receptor density (55 sites/μm^2). The findings suggest that the nature of E-selectin bond(s) engaged to initiate cell rolling does not change dramatically with changing shear stress provided the site density is 80 sites/μm^2 or larger, i.e., a similar number of bonds are required to initiate rolling over the range of shear. 3) We observed that the on-rates of selectins follow in the following sequence: L-selectin (1000/s) > P-selectin (300–450/s) > E-selectin (100–250/s).

The distance that the cell rolls on the flow chamber substrate before progressing to arrest is inversely related to the kinetics of integrin activation. We observed that, in our experiments, where cell activation is tyrosine kinase mediated, the time required for cell arrest was fairly constant over the range of shear stresses from 294 s at 0.5 dyn/cm^2 to 362 s at 2 dyn/cm^2. These time values are ~2–3 times the values reported elsewhere (Divietro et al., 2001). In the other system, neutrophils rolled on a substrate composed of P-selectin, ICAM-1, and immobilized IL-8. Activation of neutrophils by immobilized IL-8 via a G-protein-coupled mechanism resulted in firm arrest. Differences between our results and those reported by Divietro et al. (2001) could be due to a variety of factors including differences in the neutrophil activation mechanism.

In summary, the paper provides a novel analysis tool to convert cell rolling and adhesion data into adhesion frequencies and probabilities. We propose that such an analysis of flow chamber data may yield a better understanding of the role of shear forces in modulating receptor–ligand binding rates and biophysics.

APPENDIX I: VELOCITY PROFILE SURROUNDING A SURFACE-ADHERENT CELL

Cells bound to the flow chamber substrate may affect the rolling cell density both by presenting additional ligands for secondary attachment and by altering the local hydrodynamic environment. We estimated here, analytically, the extent to which a bound cell can alter the local flow profile. First, we consider the simple case of flow near a substrate in the absence of any surface-bound cell. Here, the fluid velocity, v, varies approximately linearly with distance, y, from the wall. The velocity at a height equal to one cell radius from the wall is thus $v_0 \approx \gamma_w a$. This flow near the wall is a creeping flow because the Reynolds number ($= 2av_0\rho/\mu$) is far less than 0.1. In the second case, we consider the case of flow around a substrate-bound sphere. Neglecting hydrodynamic wall effects, the creeping flow around the sphere can be expressed as a superposition of two simple flows (Fig. A1 *A*)(Aris, 1989): 1) A uniform creeping flow with velocity v_0 ($= \gamma_w a$) around a rigid sphere of radius a., and 2) a linear shear flow centered around the center of the bound sphere with $v = 0$ at $y = a$, and $v = -\gamma_w a$ at $y = 0$.

The first flow is the classic flow first treated by Stokes (Bird et al., 1961), according to which the fluid velocity at a radial distance r (where $r > a$) from the center of the sphere is

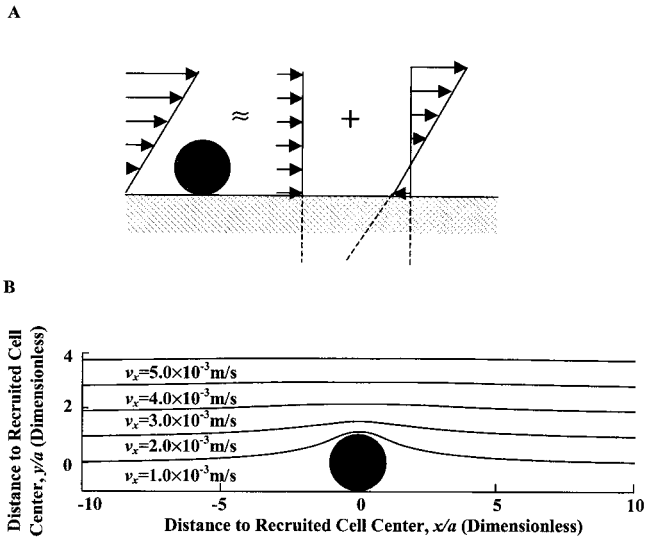

Figure A1 Local change in flow due to substrate-adherent cell. (*A*) Linear flow along the substrate was approximated to equal the sum of two flows: a constant velocity ($v = v_0 \approx \gamma_w a$) and a linear shear about the center of the cell ($v = G \cdot y$). Hydrodynamic wall effects were neglected. Local velocities calculated by solution of Navier-Stokes equation in the two cases were summed to obtain net velocity. (*B*) Contour plot lines with equal velocity in the x-direction (v_x) is used to depict the flow profile around a substrate-bound cell. The disturbance to linear shear flow is prominent up to a distance of 2.5 cell diameters away from the adherent cell, along both the length and height of the flow chamber.

$$\begin{aligned} v_r &= v_0\left[1 - \frac{3}{2}\left(\frac{a}{r}\right) + \frac{1}{2}\left(\frac{a}{r}\right)^3\right]\cos\theta, \\ v_0 &= -v_0\left[1 - \frac{3}{4}\left(\frac{a}{r}\right) - \frac{1}{4}\left(\frac{a}{r}\right)^3\right]\sin\theta, \\ v_\phi &= 0. \end{aligned} \qquad \text{(A1)}$$

For the second case, the velocity gradient tensor **G** for linear shear is given by

$$\mathbf{G} = \begin{bmatrix} 0 & 0 & 0 \\ 0 & 0 & \gamma_w \\ 0 & 0 & 0 \end{bmatrix}. \qquad \text{(A2)}$$

The governing equations for this flow include the Navier–Stokes equation for creeping flow and the continuity equation (Eq. A3). These equations written in terms of a position vector, **y**, are

$$\begin{aligned} &\nabla P = \mu\nabla^2 v \\ &\nabla \cdot v = 0, \quad \text{for all} \quad |y| > a \\ &\text{BC1} \quad v = 0 \quad \text{at} \quad |y| = a \\ &\text{BC2} \quad v = \mathbf{G}\cdot\mathbf{y} \quad \text{at} \quad |y| \to \infty \end{aligned} \qquad \text{(A3)}$$

The solution for the velocity expression is given by Eq. A4 (Batchelor, 1967), where $r = |\mathbf{y}|$ denotes the distance from the center of the sphere,

$$\nu = \mathbf{G}\cdot\mathbf{y}\left[1 - \frac{a^5}{r^5}\right] + (\mathbf{G}:\mathbf{yy})\mathbf{y}\left\{-\frac{5}{2}\frac{a^3}{r^5}\left[1 - \left(\frac{a}{r}\right)^2\right]\right\}. \tag{A4}$$

Summing Eqs. A1 and A4, and expressing the solution in Cartesian coordinates, we obtain the fluid velocity at any position (x, y, z) around the rigid sphere of radius a (where $x, y, z \geq a$):

$$\nu_x = C_1 + C_2 x + \frac{x^2}{r^2}(C_3 + C_4) - C_4,$$

$$\nu_y = C_2 y + \frac{xy}{r^2}(C_3 + C_4), \tag{A5}$$

$$\nu_z = C_2 y + \frac{xz}{r^2}(C_3 + C_4).$$

Here $C_1 = \gamma_w y(1 - (a/r)^5)$, $C_2 = \gamma_w xy(-5/2 \times (a/r)^3 + 5/2 \times (a/r)^5)$, $C_3 = v_0(1 - 3/2 \times (a/r) + 1/2 \times (a/r)^3)$, and $C_4 = -v_0(1 - 3/4 \times (a/r) - 1/4 \times (a/r)^3)$. Figure A1 *B* depicts contour lines of equal fluid velocity in x direction (v_x) around a surface-bound sphere as described by Eq. A5. It is apparent that the surface-bound cell causes a disturbance to the local flow. To quantify the magnitude of this disturbance, we estimated the ratio of the local shear rate in the presence of the cell to that in the absence of the cell (data not shown). We observed that the local shear rate is altered by greater than 5% along both the length and height of the flow chamber, up to a distance of ~2.5 cell diameters away from the surface-bound cell. We note that we have neglected the hydrodynamic wall effects in our calculations. These effects retard the disturbance created by the bound sphere, i.e., make it decay more rapidly with distance than the unbounded-fluid disturbance considered here. Therefore, our calculation represents an upper bound on the hydrodynamic effects of a bound sphere. The disturbance to flow is independent of the applied shear rate because of the linearity of the creeping flow problem. Based on this calculation, it may be expected that, at any shear rate, a surface-adherent cell may influence the nature of secondary tethering up to a distance of 2.5 cell diameters away.

We are grateful to Dr. Johannes M. Nitsche and Harish Shankaran for valuable discussions.

We also acknowledge grant support from the Whitaker Foundation and the National Institutes of Health (HL63014). Computer code for this work is available from the corresponding author.

REFERENCES

Abbassi, O., T. K. Kishimoto, L. V. McIntire, D. C. Anderson, and C. W. Smith. 1993. E-selectin supports neutrophil rolling in vitro under conditions of flow. *J. Clin. Invest.* 92:2719–2730.

Alon, R., D. A. Hammer, and T. A. Springer. 1995. Lifetime of the P-selectin–carbohydrate bond and its response to tensile force in hydrodynamic flow. *Nature.* 374:539–542.

Alon, R., R. C. Fuhlbrigge, E. B. Finger, and T. A. Springer. 1996. Interactions through L-selectin between leukocytes and adherent leukocytes nucleate rolling adhesions on selectins and VCAM-1 in shear flow. *J. Cell Biol.* 135:849–865.

Aris, R. 1989. Vectors, Tensors, and the Basic Equations of Fluid Mechanics. Dover Publications, New York.

Batchelor, G. K. 1967. An Introduction to Fluid Dynamics. Cambridge University Press, Cambridge, UK. 248–250.

Bell, D. N., S. Spain, and H. L. Goldsmith. 1989. Adenosine diphosphate-induced aggregation of human platelets in flow through tubes. I. Measurement of concentration and size of single platelets and aggregates. *Biophys. J.* 56:817–828.

Bird, R. B., W. E. Stewart, and E. Lightfoot. 1961. Transport Phenomena. John Wiley, New York. 56–57.

Brenner, H. 1961. The slow motion of a sphere through a viscous fluid towards a plane surface. *Chem. Eng. Sci.*16:242–251.

Chang, K. C., and D. A. Hammer. 1999. The forward rate of binding of surface-tethered reactants: effect of relative motion between two surfaces. *Biophys. J.* 76:1280–1292.

Davis, J. M., and J. C. Giddings. 1985. Influence of wall-retarded transport of retention and plate height in field-flow fractionation. *Sep. Sci. Techn.* 20:699–724.

Diacovo, T. G., S. J. Roth, J. M. Buccola, D. F. Bainton, and T. A. Springer. 1996. Neutrophil rolling, arrest, and transmigration across activated, surface-adherent platelets via sequential action of P-selectin and the beta 2-integrin CD11b/CD18. *Blood.* 88:146–157.

Divietro, J. A., M. J. Smith, B. R. Smith, L. Petruzzelli, R. S. Larson, and M. B. Lawrence. 2001. Immobilized IL-8 triggers progressive activation of neutrophils rolling in vitro on P-selectin and intercellular adhesion molecule-1. *J. Immunol.* 167:4017–4025.

Eriksson, E. E., X. Xie, J. Werr, P. Thoren, and L. Lindbom. 2001. Importance of primary capture and L-selectin-dependent secondary capture in leukocyte accumulation in inflammation and atherosclerosis in vivo. *J. Exp. Med.* 194:205–218.

Erlandsen, S. L., S. R. Hasslen, and R. D. Nelson. 1993. Detection and spatial distribution of the beta 2 integrin (Mac-1) and L-selectin (LECAM-1) adherence receptors on human neutrophils by high-resolution field emission SEM. *J. Histochem. Cytochem.* 41:327–333.

Evans, E., A. Leung, D. Hammer, and S. Simon. 2001. Chemically distinct transition states govern rapid dissociation of single L-selectin bonds under force. *Proc. Natl. Acad. Sci. U.S.A.* 98:3784–3789.

Felding-Habermann, B., R. Habermann, E. Saldivar, and Z. M. Ruggeri. 1996. Role of beta3 integrins in melanoma cell adhesion to activated platelets under flow. *J. Biol. Chem.* 271:5892–5900.

Goldman, A. J., R. G. Cox, and H. Brenner. 1967. Slow viscous motion of a sphere parallel to a plane wall—II. Couette flow. *Chem. Eng. Sci.* 20:653–660.

Gopalan, P. K., C. W. Smith, H. Lu, E. L. Berg, L. V. McIntire, and S. I. Simon. 1997. Neutrophil CD18-dependent arrest on intercellular adhesion molecule 1 (ICAM-1) in shear flow can be activated through L-selectin. *J. Immunol.* 158:367–375.

Graves, B. J., R. L. Crowther, C. Chandran, J. M. Rumberger, S. Li, K. S. Huang, D. H. Presky, P. C. Familletti, B. A. Wolitzky, and D. K. Burns. 1994. Insight into E-selectin/ligand interaction from the crystal structure and mutagenesis of the lec/EGF domains. *Nature.* 367:532–538.

Guyer, D. A., K. L. Moore, E. B. Lynam, C. M. Schammel, S. Rogelj, R. P. McEver, and L. A. Sklar. 1996. P-selectin glycoprotein ligand-1 (PSGL-1) is a ligand for L-selectin in neutrophil aggregation. *Blood.* 88:2415–2421.

King, M. R., and D. A. Hammer. 2001. Multiparticle adhesive dynamics: hydrodynamic recruitment of rolling leukocytes. *Proc. Natl. Acad. Sci. U.S.A.* 98:14919–14924.

Lawrence, M. B., L. V. McIntire, and S. G. Eskin. 1987. Effect of flow on polymorphonuclear leukocyte/endothelial cell adhesion. *Blood.* 70: 1284–1290.

Mitchell, D. J., P. Li, P. H. Reinhardt, and P. Kubes. 2000. Importance of L-selectin-dependent leukocyte–leukocyte interactions in human whole blood. *Blood.* 95:2954–2959.

Mohamed, N., M. A. Teeters, J. M. Patti, M. Hook, and J. M. Ross. 1999. Inhibition of *Staphylococcus aureus* adherence to collagen under dynamic conditions. *Infect. Immun.* 67:589–594.

Moore, K. L., K. D. Patel, R. E. Bruehl, F. Li, D. A. Johnson, H. S. Lichenstein, R. D. Cummings, D. F. Bainton, and R. P. McEver. 1995. P-selectin glycoprotein ligand-1 mediates rolling of human neutrophils on P-selectin. *J. Cell Biol.* 128:661–671.

Munn, L. L., R. J. Melder, and R. K. Jain. 1994. Analysis of cell flux in the parallel plate flow chamber: implications for cell capture studies. *Biophys. J.* 67:889–895.

Myszka, D. G., X. He, M. Dembo, T. A. Morton, and B. Goldstein. 1998. Extending the range of rate constants available from BIACORE: interpreting mass transport-influenced binding data. *Biophys. J.* 75:583–594.

Neelamegham, S., L. L. Munn, and K. Zygourakis. 1997a. A model for the kinetics of homotypic cellular aggregation under static conditions. *Biophys. J.* 72:51–64.

Neelamegham, S., A. D. Taylor, J. D. Hellums, M. Dembo, C. W. Smith, and S. I. Simon. 1997b. Modeling the reversible kinetics of neutrophil aggregation under hydrodynamic shear. *Biophys. J.* 72:1527–1540.

Neelamegham, S., A. D. Taylor, A. R. Burns, C. W. Smith, and S. I. Simon. 1998. Hydrodynamic shear shows distinct roles for LFA-1 and Mac-1 in neutrophil adhesion to intercellular adhesion molecule-1. *Blood.* 92: 1626–1638.

Patel, K. D., and R. P. McEver. 1997. Comparison of tethering and rolling of eosinophils and neutrophils through selectins and P-selectin glycoprotein ligand-1. *J. Immunol.* 159:4555–4565.

Patil, V. R., C. J. Campbell, Y. H. Yun, S. M. Slack, and D. J. Goetz. 2001. Particle diameter influences adhesion under flow. *Biophys. J.* 80: 1733–1743.

Puri, K. D., E. B. Finger, and T. A. Springer. 1997. The faster kinetics of L-selectin than of E-selectin and P-selectin rolling at comparable binding strength. *J. Immunol.* 158:405–413.

Rinker, K. D., V. Prabhakar, and G. A. Truskey. 2001. Effect of contact time and force on monocyte adhesion to vascular endothelium. *Biophys. J.* 80:1722–1732.

Schneck, D. 2000. Cardiovascular mechanics. *In* Introduction to Biomedical Engineering. J. Enderle, S. Blanchard, and J. Bronzino, editors. Academic Press, New York. 473.

Shankaran, H., and S. Neelamegham. 2001. Nonlinear flow affects hydrodynamic forces and neutrophil adhesion rates in cone-plate viscometers. *Biophys. J.* 80:2631–2648.

Shao, J. Y., H. P. Ting-Beall, and R. M. Hochmuth. 1998. Static and dynamic lengths of neutrophil microvilli. *Proc. Natl. Acad. Sci. U.S.A.* 95:6797–6802.

Simon, S. I., J. D. Chambers, E. Butcher, and L. A. Sklar. 1992. Neutrophil aggregation is beta 2-integrin- and L-selectin-dependent in blood and isolated cells. *J. Immunol.* 149:2765–2771.

Simon, S. I., Y. Hu, D. Vestweber, and C. W. Smith. 2000. Neutrophil tethering on E-selectin activates beta 2 integrin binding to ICAM-1 through a mitogen-activated protein kinase signal transduction pathway. *J. Immunol.* 164:4348–4358.

Springer, T. A. 1990. Adhesion receptors of the immune system. *Nature.* 346:425–434.

Szabo, A., K. Schulten, and Z. Schulten. 1980. First passage time approach to diffusion controlled reactions. *J. Chem. Phys.* 72:4350–4357.

Taylor, A. D., S. Neelamegham, J. D. Hellums, C. W. Smith, and S. I. Simon. 1996. Molecular dynamics of the transition from L-selectin- to beta 2- integrin-dependent neutrophil adhesion under defined hydrodynamic shear. *Biophys. J.* 71:3488–3500.

Walcheck, B., K. L. Moore, R. P. McEver, and T. K. Kishimoto. 1996. Neutrophil–neutrophil interactions under hydrodynamic shear stress involve L-selectin and PSGL-1. A mechanism that amplifies initial leukocyte accumulation of P-selectin in vitro. *J. Clin. Invest.* 98: 1081–1087.